



## OPEN Numerical modeling and simulation of stochastic fractional order model for COVID-19 infection in Mittag–Leffler kernel

Muhammad Altaf Khan<sup>1,2,3,4,9</sup>✉, Zain Ul Abadin Zafar<sup>5,9</sup>, Irfan Ahmad<sup>6,9</sup>, Nurulfiza Mat Isa<sup>2,8,9</sup> & Ebraheem Alzahrani<sup>7,9</sup>

In this work, we develop and analyze a fractional-order stochastic model for COVID-19 transmission, incorporating the effects of vaccination. The model is formulated using the Atangana–Baleanu fractional derivative in the Caputo sense, which captures memory and hereditary properties of disease transmission more accurately than classical derivatives. We first examine the positivity and boundedness of the deterministic fractional model and determine its equilibrium points. The model is then extended to a fractional stochastic differential equation (FSDE) to account for random fluctuations and uncertainties in disease dynamics. We establish the existence and uniqueness of solutions for the FSDE model using stochastic analysis techniques. To numerically solve the FSDE, we develop a novel numerical scheme that accommodates the non-local nature of the Atangana–Baleanu derivative. The real data of COVID-19 in Pakistan have been used to estimate the model parameters. Numerical simulations are presented for both the deterministic fractional model and its stochastic counterpart. These simulations illustrate the impact of the fractional-order parameter on disease dynamics, showing how different orders influence the rate of infection and convergence to equilibrium. Additionally, we analyze scenarios under varying parameter values to explore conditions for disease elimination, highlighting the role of vaccination and stochasticity. Our findings demonstrate that fractional stochastic modeling provides deeper understanding of COVID-19 transmission dynamics and can be a valuable tool in assessing control strategies under uncertainty. The originality of this work stems from the integration of Atangana–Baleanu fractional derivatives with stochastic modeling, supported by a new numerical solution method providing a more realistic and flexible approach to modeling COVID-19 transmission under uncertainty.

The COVID-19 infection shook the world economy and human health. A lot of infected cases have been reported around the globe, and at the same time, a high number of deaths have been reported throughout the world. As the infection continues to spread within the human population, different variants of COVID-19 have been reported in many parts of the world, where one variant is found to be more severe than the other. Researchers and scientists are always exploring vaccine development to combat coronavirus disease. Different types of COVID-19 vaccines have been developed with different names for the disease curtail. After the vaccination of the people in each country, the number of infected people dropped day by day, and after some time, the cases have almost reached to minimum.

The COVID-19 infection has been identified in nearly all parts of the world, resulting in a significant number of cases and fatalities. Various mathematical models or other theoretical approaches are presented to highlight

<sup>1</sup>Department of Mathematics, Saveetha School of Engineering, SIMATS, Saveetha University, 602105 Chennai, Tamil Nadu, India. <sup>2</sup>Laboratory of Vaccine and Biomolecules, Institute of Bioscience, Universiti Putra Malaysia, UPM, 43400 Serdang, Selangor, Malaysia. <sup>3</sup>School of Health and Environmental Science, Korea University, 02841 Seoul, South Korea. <sup>4</sup>Faculty of Natural and Agricultural Sciences, University of the Free State, 9300 Bloemfontein, South Africa. <sup>5</sup>Department of Mathematics, Faculty of Science and Technology, University of Central Punjab, Lahore, Pakistan. <sup>6</sup>Department of Clinical Laboratory Sciences, College of Applied Medical Sciences, King Khalid University, Abha, Saudi Arabia. <sup>7</sup>Department of Mathematics, Faculty of Science, King Abdulaziz University, Jeddah, Saudi Arabia. <sup>8</sup>Department of Cell and Molecular Biology, Faculty of Biotechnology and Biomolecular Sciences, Universiti Putra Malaysia, 43400 Serdang, Selangor, Malaysia. <sup>9</sup>Muhammad Altaf Khan, Zain Ul Abadin, Irfan Ahmad, Nurulfiza Mat Isa and Ebraheem Alzahrani: These authors contributed equally to this work. ✉email: altafdir@gmail.com

the COVID-19 issue<sup>1-5</sup>. For example, the authors in<sup>1</sup> considered the COVID-19 model in fractional derivative using the impact of public health awareness. In<sup>2</sup>, the authors considered the COVID-19 model in fractional derivatives by considering the Atangana-Baleanu derivative concept. The impact of public sentiments on the modeling of COVID-19 infection dynamics is described in<sup>3</sup>. The COVID-19 model employed to investigate the early reported cases using a fractional-order approach is presented in<sup>4</sup>, while the COVID-19 model with optimal control interventions based on real data is given in<sup>5</sup>. The literature regarding the mathematical models that were developed to find out the disease propagation, the early control of the disease, and to determine their basic reproduction number. Some simple mathematical models were also presented to determine the basic reproduction and some statistical approaches were used to show the possible details of the infected cases and the future trend of the disease. One important thing that we saw in the COVID-19 cases was the peak of the infected cases, where one can determine the peak of the cases using statistical or mathematical modeling approaches to determine/predict the possible peak and the days required for the disease elimination based on the specific data used.

Various mathematical models utilizing fractional derivatives have been reported to investigate disease dynamics; see, for example,<sup>6-9</sup>. The concept of stochastic differential equations has been applied to analyze the coronavirus disease, as presented in<sup>10</sup>. The real cases of the coronavirus in the UAE have been used to obtain parameters with realistic values, and further to obtain results for curtailing the infection in the UAE. A mathematical model that incorporates the assumptions of treatment of the infected individuals of COVID-19 has been explored in<sup>11</sup>. A mathematical model that focuses on vaccination strategies for coronavirus infection is discussed in<sup>12</sup>. In<sup>13</sup>, the authors analyzed COVID-19 infection data from India using a Caputo–Fabrizio derivative model. A cholera infection model in terms of fractional derivative is discussed in<sup>14</sup>. A monkeypox disease model considering the fractional derivative has been used in<sup>15</sup>. A coronavirus infection under the environmental contamination has been considered in<sup>16</sup>. Some more work on fractional order models, we can refer the readers to see<sup>17-20</sup>.

Mathematical models that are designed in terms of stochastic environments are considered useful for the prediction of disease and spread, as they account for uncertainty and randomness in biological mathematical models. The deterministic mathematical systems usually have some constraints<sup>21</sup>. Disease extinction probability cannot be taken into consideration by a deterministic model<sup>22</sup>. In order to depict random fluctuations in physiological parameters and natural processes like cell development and death, this model incorporates stochastic components. Particularly in human viral infections, random variations in environmental factors like temperature, humidity, and precipitation can greatly influence the transmission of the disease. These stochastic effects capture the impact of shifting environmental variables in biological models. A fractional stochastic mathematical model that is designed to study the media awareness in disease spread has been explored in<sup>23</sup>. An SIR fractional model in a stochastic environment has been analyzed in<sup>24</sup>. A fractal-fractional stochastic coronavirus model incorporating the vaccination effects has been explored in<sup>25</sup>. The dynamics of Ebola infection in terms of stochastic fractional environments have been analyzed by the authors in<sup>26</sup>. The combined effects model with stochastic and fractional calculus to understand the coronavirus infection has been explored in<sup>27</sup>.

In this investigation, the COVID-19 infection model with vaccination in stochastic fractional differential equations is considered. The model is first presented with integer-order derivatives, subsequently reformulated in terms of the ABC derivative, and later generalized to fractional stochastic differential equations. We provide the EU of the system, their positivity and boundedness, and a non-negative solution. The sensitivity analysis has been performed by using the PRCC method and provided comprehensive details about the sensitive parameters that have an effect on the disease model. A numerical solution for the model with an effective scheme has been shown. Numerical simulations are performed and analyzed to evaluate the influence of different parameter values on disease control.

## Mathematical model

This section presents the mathematical modeling of the COVID-19 infection model in integer order derivative. We partition the total population into six distinct compartments: susceptible individuals  $S(t)$ , representing unvaccinated persons at risk of infection; vaccinated individuals  $V(t)$ ; exposed individuals  $E(t)$ , who are infected but not yet infectious; asymptomatic infectious individuals  $A(t)$ ; symptomatic infectious individuals  $I(t)$ ; and recovered individuals  $R(t)$ . The overall population at time  $t$  is therefore expressed as

$$N(t) = S(t) + V(t) + E(t) + A(t) + I(t) + R(t).$$

Vaccinated individuals are initially protected from infection due to the immunological response induced by the vaccine. However, as vaccine efficacy wanes over time, some vaccinated individuals may become susceptible to the virus again. On the basis of these assumptions, we formulate a system of nonlinear ordinary differential equations to characterize the transmission dynamics of the virus across the defined compartments<sup>28</sup>.

$$\begin{cases} \frac{dS}{dt} = -\frac{(a_1I + a_2A)S}{N} - S(\mu + \omega) + \kappa R + \theta V + \Pi, \\ \frac{dV}{dt} = \omega S - (1 - \psi)\frac{(a_1I + a_2A)V}{N} - (\theta + \mu)V, \\ \frac{dE}{dt} = -(\delta + \mu)E + \frac{(a_1I + a_2A)S}{N} + (1 - \psi)\frac{(a_1I + a_2A)V}{N}, \\ \frac{dA}{dt} = \delta qE - (\mu + \rho_1)A, \\ \frac{dI}{dt} = -(\mu + d + \rho)I + (1 - q)\delta E, \\ \frac{dR}{dt} = -(\kappa + \mu)R + \rho I + \rho_1 A. \end{cases} \quad (1)$$

According to the initial assumption

$$S(0) = S_0 > 0, V(0) = V_0 \geq 0, E(0) = E_0 \geq 0, A(0) = A_0 \geq 0, I(0) = I_0 \geq 0, R(0) = R_0 \geq 0. \quad (2)$$

The system is characterized by several key parameters that govern its dynamics. The recruitment rate of the healthy people is given by  $\Pi$ , while  $\mu$  denotes the natural death rate. Disease propagates when susceptible persons are exposed to infectious contacts through either symptomatic or asymptomatic transmission routes, characterized by the rates  $a_1$  and  $a_2$ , respectively. Vaccination of susceptible individuals is administered at a rate  $\omega$ , while waning vaccine immunity occurs at a rate  $\theta$ . Recovered individuals may experience natural loss of immunity, represented by the rate  $\kappa$ .

Given the absence of a perfect coronavirus vaccine, the parameter  $\psi$  accounts for vaccine efficacy. The incubation period following exposure is denoted by  $\delta$ . The movement of exposed individuals into the asymptomatic compartment  $A(t)$  occurs with rate  $q\delta$ . Individuals who develop symptoms move to the symptomatic infectious compartment  $I(t)$  at a rate  $(1 - q)\delta$ . The recovery rate for asymptomatic infections is denoted by  $\rho_1$ , while that for symptomatic infections is represented by  $\rho$ . Disease-induced mortality at the symptomatic stage is represented by the parameter  $d$ . Coronavirus has been responsible for significant mortality worldwide.

### Formulation of fractional model and related definitions

The following basic definitions will be utilized in developing the fractional-order model.

**Definition 1** The Atangana-Baleanu derivative in Caputo sense ( $\mathbb{ABC}$ ) and their respective fractional integral is hereby presented:

$${}^{\mathbb{ABC}}\mathcal{D}_t^\zeta(\phi(t)) = \frac{\mathbb{ABC}(\zeta)}{(1 - \zeta)} \int_0^t \phi'(\theta) E_\zeta \left[ \frac{\zeta(t - \theta)^\zeta}{\zeta - 1} \right] d\theta,$$

$\mathbb{ABC}(\zeta)$  is the normalization function which satisfies  $\mathbb{ABC}(1) = \mathbb{ABC}(0) = 1$ . The AB arbitrary integral of order  $\zeta$  for a function  $\phi$  is given by

$${}^{\mathbb{ABC}}\mathcal{I}_t^\zeta(\phi(t)) - \frac{1 - \zeta}{\mathbb{ABC}(\zeta)}\phi(t) = \zeta(\mathbb{ABC}(\zeta)\Gamma(\zeta))^{-1} \int_0^t (t - \theta)^{\zeta-1} \phi(\theta) d\theta,$$

where  $0 < \zeta \leq 1$ ,  $t \in [0, \infty)$ , and  $\phi(t)$  defines a differentiable function over the interval  $[0, \infty)$  such that  $\phi' \in L^1(0, \infty)$ ,  $E_\zeta$  is the Mittag-Leffler function (MLF).

Converting an integer-order epidemiological model to a fractional-order model offers several key advantages. Fractional models incorporate memory and hereditary properties, making them more suitable for capturing the long-term dynamics and history-dependent behavior of infectious diseases. Unlike integer-order models, which assume that the future state depends only on the present, fractional models account for the influence of past states, leading to more accurate and realistic descriptions of disease spread. This enhanced modeling capability often results in better fitting of real-world data and improved predictions, especially in complex systems like COVID-19, where disease transmission is influenced by delayed responses and long-term immunity effects. Therefore, the classical differential operator given in (1) is replaced by the Atangana-Baleanu (AB) fractional derivative.

$$\begin{cases} {}_0^{\text{ABC}}D_t^\zeta S(t) = \Pi - \frac{(a_1 I + a_2 A)S}{N} - (\mu + \omega)S + \kappa R + \theta V, \\ {}_0^{\text{ABC}}D_t^\zeta V(t) = \omega S - (1 - \psi) \frac{(a_1 I + a_2 A)V}{N} - (\theta + \mu)V, \\ {}_0^{\text{ABC}}D_t^\zeta E(t) = \frac{(a_1 I + a_2 A)S}{N} + (1 - \psi) \frac{(a_1 I + a_2 A)V}{N} - (\delta + \mu)E, \\ {}_0^{\text{ABC}}D_t^\zeta A(t) = \delta q E - (\mu + \rho_1)A, \\ {}_0^{\text{ABC}}D_t^\zeta I(t) = -(d + \mu + \rho)I + \delta(1 - q)E, \\ {}_0^{\text{ABC}}D_t^\zeta R(t) = \rho_1 A + \rho I - (\mu + \kappa)R, \end{cases} \tag{3}$$

with the associated non-negative initial conditions,

$$S(0) = S_0 > 0, V(0) = V_0 \geq 0, E(0) = E_0 \geq 0, A(0) = A_0 \geq 0, I(0) = I_0 \geq 0, R(0) = R_0 \geq 0.$$

Before analyzing model (3), we first verify its biological feasibility by examining the existence, uniqueness, and positivity of solutions, as well as the invariance of the feasible region in  $\mathbb{R}_+^6$ . The feasible region is defined as

$$\mathbb{R}_+^6 = \left\{ (S, V, E, A, I, R) \in \mathbb{R}^6 \mid S, V, E, A, I, R \geq 0 \right\}.$$

In the next subsection, this condition will be elaborated.

### Existence and Uniqueness (EU)

Here, we establish the EU results for the model (3) in non-integer order derivative in ABC sense. For this purpose, we present the following result:

**Theorem 1** <sup>29</sup> *There exists a unique solution to the fractional differential equation*

$${}_0^{\text{ABC}}D_t^\zeta x(t) = f(t), \tag{4}$$

which can be obtained through the inverse Laplace transform and the convolution theorem, and is given by

$$x(t) - \mathcal{A}f(t) = \mathcal{B} \int_0^t f(s) (t - s)^{\zeta-1} ds. \tag{5}$$

Now, we use Theorem 1 to transform the system (3) into a Volterra-type integral equation, given by:

$$\begin{cases} S(t) - S(0) - \mathcal{A}H_{11}(S, t) = \mathcal{B} \int_0^t H_{11}(S, s) (t - s)^{\zeta-1} ds, \\ V(t) - V(0) - \mathcal{A}H_{12}(V, t) = \mathcal{B} \int_0^t H_{12}(V, s) (t - s)^{\zeta-1} ds, \\ E(t) - E(0) - \mathcal{A}H_{13}(E, t) = \mathcal{B} \int_0^t H_{13}(E, s) (t - s)^{\zeta-1} ds, \\ A(t) - A(0) - \mathcal{A}H_{14}(A, t) = \mathcal{B} \int_0^t H_{14}(A, s) (t - s)^{\zeta-1} ds, \\ I(t) - I(0) - \mathcal{A}H_{15}(I, t) = \mathcal{B} \int_0^t H_{15}(I, s) (t - s)^{\zeta-1} ds, \\ R(t) - R(0) - \mathcal{A}H_{16}(R, t) = \mathcal{B} \int_0^t H_{16}(R, s) (t - s)^{\zeta-1} ds. \end{cases} \tag{6}$$

where  $\mathcal{A} = \frac{1-\zeta}{{}_0^{\text{ABC}}\Gamma(\zeta)}$  and  $\mathcal{B} = \frac{\zeta}{\Gamma(\zeta){}_0^{\text{ABC}}\Gamma(\zeta)}$ . Also,

$$\begin{cases} H_{11}(S, t) = \Pi - \frac{(a_1 I + a_2 A)S}{N} - (\mu + \omega)S + \kappa R + \theta V, \\ H_{12}(V, t) = \omega S - \frac{(1 - \psi)(a_1 I + a_2 A)V}{N} - (\theta + \mu)V, \\ H_{13}(E, t) = \frac{(a_1 I + a_2 A)S}{N} + \frac{(1 - \psi)(a_1 I + a_2 A)V}{N} - (\delta + \mu)E, \\ H_{14}(A, t) = -(\mu + \rho_1)A + \delta q E, \\ H_{15}(I, t) = -(\mu + d + \rho)I + (1 - q)\delta E, \\ H_{16}(R, t) = -(\kappa + \mu)R + \rho I + \rho_1 A. \end{cases} \tag{7}$$

To prove that the kernels  $H_{1i}$ , for  $i, 1$  to  $6$  satisfy the Lipschitz condition, we have to show that these kernels are Lipschitz continuous with respect to the given functions. Consider that  $S, \bar{S}, V, \bar{V}, A, \bar{A}, E, \bar{E}, I, \bar{I}, R, \bar{R}$  representing bounded functions, such that

$$\max \left\{ S, \bar{S}, V, \bar{V}, A, \bar{A}, E, \bar{E}, I, \bar{I}, R, \bar{R} \right\} < \beta.$$

For  $H_{11}(S, t)$  and  $H_{11}(\bar{S}, t)$ , the following inequality holds,

$$\begin{aligned} \|H_{11}(t, S) - H_{11}(t, \bar{S})\| &= \left\| -\frac{(a_1 I + a_2 A)(S - \bar{S})}{N} - (\mu + \omega)(S - \bar{S}) \right\|, \\ &\leq \frac{(a_1 + a_2)\beta}{N} \|S - \bar{S}\| + (\mu + \omega)\|S - \bar{S}\|, \\ &\leq \left( \frac{(a_1 + a_2)\beta}{N} + (\mu + \omega) \right) \|S - \bar{S}\|, \leq \gamma_1 \|S - \bar{S}\|. \end{aligned} \tag{8}$$

where  $\gamma_1 = \left( \frac{(a_1 + a_2)\beta}{N} + (\mu + \omega) \right)$ . Follow the results given in<sup>30</sup> (see Theorem 1), the kernel  $H_{11}(t, S)$  satisfies the Lipschitz condition. In a similar way, the following inequalities can be obtained:

$$\begin{aligned} \|H_{12}(t, V) - H_{12}(t, \bar{V})\| &\leq \gamma_2 \| -\bar{V} + V \|, \\ \|H_{13}(t, E) - H_{13}(t, \bar{E})\| &\leq \gamma_3 \| -\bar{E} + E \|, \\ \|H_{14}(t, A) - H_{14}(t, \bar{A})\| &\leq \gamma_4 \| -\bar{A} + A \|, \\ \|H_{15}(t, I) - H_{15}(t, \bar{I})\| &\leq \gamma_5 \| -\bar{I} + I \|, \\ \|H_{16}(t, R) - H_{16}(t, \bar{R})\| &\leq \gamma_6 \| -\bar{R} + R \|, \end{aligned} \tag{9}$$

where  $\gamma_2 = \frac{(1-\psi)(a_1+a_2)\beta}{N} + (\mu + \theta)$ ,  $\gamma_3 = \mu + \delta$ ,  $\gamma_4 = \mu + \rho_1$ ,  $\gamma_5 = \mu + \rho + d$  and  $\gamma_6 = \kappa + \mu$ . Thus, for all kernels  $H_{1i}$ ,  $i = 1, 2, 3, \dots, 6$ , the Lipschitz condition holds. Furthermore, we use the fixed point theory to obtain the existence of the solution of the system (3). The recursive formulation of the Eq. (6) is shown by the following expressions,

$$\begin{cases} S_n(t) - \mathcal{A}H_{11}(S_{n-1}, t) = \mathcal{B} \int_0^t (t-s)^{\zeta-1} H_{11}(S_{n-1}, s) ds, \\ V_n(t) - \mathcal{A}H_{12}(V_{n-1}, t) = \mathcal{B} \int_0^t (t-s)^{\zeta-1} H_{12}(V_{n-1}, s) ds, \\ E_n(t) - \mathcal{A}H_{13}(E_{n-1}, t) = \mathcal{B} \int_0^t (t-s)^{\zeta-1} H_{13}(E_{n-1}, s) ds, \\ A_n(t) - \mathcal{A}H_{14}(A_{n-1}, t) = \mathcal{B} \int_0^t (t-s)^{\zeta-1} H_{14}(A_{n-1}, s) ds, \\ I_n(t) - \mathcal{A}H_{15}(I_{n-1}, t) = \mathcal{B} \int_0^t (t-s)^{\zeta-1} H_{15}(I_{n-1}, s) ds, \\ R_n(t) - \mathcal{A}H_{16}(R_{n-1}, t) = \mathcal{B} \int_0^t (t-s)^{\zeta-1} H_{16}(R_{n-1}, s) ds. \end{cases} \tag{10}$$

The appropriate initial conditions for (10) are  $S_0 = S(0), V_0 = V(0), E_0 = E(0), A_0 = A(0), I_0 = I(0)$  and  $R_0 = R(0)$ . From (10), the various expressions for the successive terms are provided as follows:

$$\begin{cases} \Phi_{1,n} = S_n(t) - S_{n-1}(t) = \mathcal{A}(H_{11}(S_{n-1}, t) - H_{11}(S_{n-2}, t)) + \mathcal{B} \int_0^t (H_{11}(S_{n-1}, s) - H_{11}(S_{n-2}, s))(t-s)^{\zeta-1} ds, \\ \Phi_{2,n} = V_n(t) - V_{n-1}(t) = \mathcal{A}(H_{12}(V_{n-1}, t) - H_{12}(V_{n-2}, t)) + \mathcal{B} \int_0^t (H_{12}(V_{n-1}, s) - H_{12}(V_{n-2}, s))(t-s)^{\zeta-1} ds, \\ \Phi_{3,n} = E_n(t) - E_{n-1}(t) = \mathcal{A}(H_{13}(E_{n-1}, t) - H_{13}(E_{n-2}, t)) + \mathcal{B} \int_0^t (H_{13}(E_{n-1}, s) - H_{13}(E_{n-2}, s))(t-s)^{\zeta-1} ds, \\ \Phi_{4,n} = A_n(t) - A_{n-1}(t) = \mathcal{A}(H_{14}(A_{n-1}, t) - H_{14}(A_{n-2}, t)) + \mathcal{B} \int_0^t (H_{14}(A_{n-1}, s) - H_{14}(A_{n-2}, s))(t-s)^{\zeta-1} ds, \\ \Phi_{5,n} = I_n(t) - I_{n-1}(t) = \mathcal{A}(H_{15}(I_{n-1}, t) - H_{15}(I_{n-2}, t)) + \mathcal{B} \int_0^t (H_{15}(I_{n-1}, s) - H_{15}(I_{n-2}, s))(t-s)^{\zeta-1} ds, \\ \Phi_{6,n} = R_n(t) - R_{n-1}(t) = \mathcal{A}(H_{16}(R_{n-1}, t) - H_{16}(R_{n-2}, t)) + \mathcal{B} \int_0^t (H_{16}(R_{n-1}, s) - H_{16}(R_{n-2}, s))(t-s)^{\zeta-1} ds. \end{cases} \quad (11)$$

and hence we have

$$\begin{aligned} S_n - \sum_{i=1}^n \Phi_{1,i}(t) = 0, \quad V_n - \sum_{i=1}^n \Phi_{2,i}(t) = 0, \quad E_n - \sum_{i=1}^n \Phi_{3,i}(t) = 0, \\ A_n - \sum_{i=1}^n \Phi_{4,i}(t) = 0, \quad I_n - \sum_{i=1}^n \Phi_{5,i}(t) = 0, \quad R_n - \sum_{i=1}^n \Phi_{6,i}(t) = 0. \end{aligned} \quad (12)$$

By using Eqs. (8) and (9), the norms of both sides of Eq. (11) can be solved. We obtain

$$\begin{cases} \|\Phi_{1,n}\| \leq \mathcal{A}\gamma_1 \|\Phi_{1,n-1}\| + \mathcal{B}\gamma_1 \int_0^t \|\Phi_{1,n-1}(s)\| (t-s)^{\zeta-1} ds, \\ \|\Phi_{2,n}\| \leq \mathcal{A}\gamma_2 \|\Phi_{2,n-1}\| + \mathcal{B}\gamma_2 \int_0^t \|\Phi_{2,n-1}(s)\| (t-s)^{\zeta-1} ds, \\ \|\Phi_{3,n}\| \leq \mathcal{A}\gamma_3 \|\Phi_{3,n-1}\| + \mathcal{B}\gamma_3 \int_0^t \|\Phi_{3,n-1}(s)\| (t-s)^{\zeta-1} ds, \\ \|\Phi_{4,n}\| \leq \mathcal{A}\gamma_4 \|\Phi_{4,n-1}\| + \mathcal{B}\gamma_4 \int_0^t \|\Phi_{4,n-1}(s)\| (t-s)^{\zeta-1} ds, \\ \|\Phi_{5,n}\| \leq \mathcal{A}\gamma_5 \|\Phi_{5,n-1}\| + \mathcal{B}\gamma_5 \int_0^t \|\Phi_{5,n-1}(s)\| (t-s)^{\zeta-1} ds, \\ \|\Phi_{6,n}\| \leq \mathcal{A}\gamma_6 \|\Phi_{6,n-1}\| + \mathcal{B}\gamma_6 \int_0^t \|\Phi_{6,n-1}(s)\| (t-s)^{\zeta-1} ds. \end{cases} \quad (13)$$

We now state the following Theorem.

**Theorem 2** Model (3) contains a specific solution if and only if we can find  $t_{max}$  such that

$$\gamma_i \mathcal{A} + \frac{t_{max}^\zeta \gamma_i}{\Gamma(\zeta) \mathbb{ABC}(\zeta)} < 1, \quad i = 1, 2, \dots, 6. \quad (14)$$

*Proof* It is assumed that  $S, V, E, A, I$  and  $R$  representing bounded functions, and also it has been proven previously that these functions also holds the Lipschitz condition. As we can see from the Eq. (13) and applying the recursive principle, the below inequalities hold:

$$\begin{cases} \|\Phi_{1,n}\| \leq \left( \mathcal{A}\gamma_1 + \frac{t^\zeta \gamma_1}{\mathbb{ABC}(\zeta)\Gamma(\zeta)} \right)^n \|S_0\|, \quad \|\Phi_{2,n}\| \leq \left( \mathcal{A}\gamma_2 + \frac{t^\zeta \gamma_2}{\mathbb{ABC}(\zeta)\Gamma(\zeta)} \right)^n \|V_0\|, \\ \|\Phi_{3,n}\| \leq \left( \mathcal{A}\gamma_3 + \frac{t^\zeta \gamma_3}{\mathbb{ABC}(\zeta)\Gamma(\zeta)} \right)^n \|E_0\|, \quad \|\Phi_{4,n}\| \leq \left( \mathcal{A}\gamma_4 + \frac{t^\zeta \gamma_4}{\mathbb{ABC}(\zeta)\Gamma(\zeta)} \right)^n \|A_0\|, \\ \|\Phi_{5,n}\| \leq \left( \mathcal{A}\gamma_5 + \frac{t^\zeta \gamma_5}{\mathbb{ABC}(\zeta)\Gamma(\zeta)} \right)^n \|I_0\|, \quad \|\Phi_{6,n}\| \leq \left( \frac{t^\zeta \gamma_6}{\mathbb{ABC}(\zeta)\Gamma(\zeta)} + \mathcal{A}\gamma_6 \right)^n \|R_0\|. \end{cases} \quad (15)$$

We establish the existence and uniqueness of the solution to (12) by analyzing the behavior of  $\|\Phi_{i,n}(t)\| \rightarrow 0$ , as  $n \rightarrow \infty$  and  $t = t_{max}$  with  $i = 1, \dots, 6$ . To demonstrate that Eq. (6) is the solution of Eq. (3), we consider the following:

$$\begin{cases} S(t) - S(0) = S_n - \Psi_{1,n}, & V(t) - V(0) = V_n - \Psi_{2,n}, \\ E(t) - E(0) = E_n - \Psi_{3,n}, & A(t) - A(0) = A_n - \Psi_{4,n}, \\ I(t) - I(0) = I_n - \Psi_{5,n}, & R(t) - R(0) = R_n - \Psi_{6,n}. \end{cases} \tag{16}$$

where  $\Psi_{i,n}(t)$ , for  $i = 1, \dots, 6$  refers to the remainder terms in the series expansions. The norm of the term  $\Psi_{1,n}(t)$  is given by,

$$\begin{aligned} \|\Psi_{1,n}(t)\| &\leq \mathcal{A} \|H_{11}(S, t) - H_{11}(S_{n-1}, t)\| + \frac{\zeta}{\mathbb{ABC}(\zeta)\Gamma(\zeta)} \int_0^t \|H_{11}(S, s) - H_{11}(S_{n-1}, s)\| (t-s)^{\zeta-1} ds, \\ &\leq \|S - S_{n-1}\| \left( \mathcal{A} + \frac{t^\zeta}{\mathbb{ABC}(\zeta)\Gamma(\zeta)} \right) \gamma_1. \end{aligned} \tag{17}$$

As one can now apply an iteration method to inequality (17) at  $t = t_{max}$ , we obtain

$$\|\Psi_{1,n}(t)\| \leq \left( \mathcal{A} + \frac{t_{max}^\zeta}{\mathbb{ABC}(\zeta)\Gamma(\zeta)} \right)^{n+1} \gamma_1^{n+1} N. \tag{18}$$

We achieve  $\|\Psi_{1,n}(t)\| \rightarrow 0$  as  $n \rightarrow \infty$ . According to laid down procedure we have  $\|\Psi_{i,n}(t)\| \rightarrow 0$ ,  $i = 2, 3, \dots, 6$ . Thus, the function that meets the requirement of Eq. (6) is the solution of Eq. (3). The fact that the solution to model Eq. (3) is now established. Consider  $S^*, V^*, E^*, A^*, I^*$  and  $R^*$  represent another set of solution for the system (3). Thus, the below relationship is satisfied:

$$S(t) - S^*(t) = \mathcal{A} \left( H_{11}(S, t) - H_{11}(S^*, t) \right) + \mathcal{B} \int_0^t \left( H_{11}(S, t) - H_{11}(S^*, t) \right) (t-s)^{\zeta-1} ds. \tag{19}$$

By applying the same procedure as in Eq. (13) and (15) to take the norm of both sides on Eq. (19), we obtain:

$$\left( 1 - \mathcal{A}\gamma_1 - \frac{\gamma_1 t^\zeta}{\mathbb{ABC}(\zeta)\Gamma(\zeta)} \right) \|S(t) - S^*(t)\| \leq 0. \tag{20}$$

We confirm that for  $t = t_{max}$  we have

$$\left( 1 - \mathcal{A}\gamma_1 - \frac{\gamma_1 t^\zeta}{\mathbb{ABC}(\zeta)\Gamma(\zeta)} \right) \geq 0. \tag{21}$$

which clearly state that  $\|S - S^*\| = 0$ . As the result, we conclude  $S = S^*$ . By using a similar approach, it can be obtained  $V = V^*, E = E^*, A = A^*, I = I^*$  and  $R = R^*$ .  $\square$

### Positivity and boundedness

Here, we determine the solution space  $(S, V, E, A, I, R)$  associated with the model (3) under non-negative initial conditions. Specifically, we focus on identifying a feasible region, denoted as  $\mathbb{R}_+^6$ , which remains positively invariant under the dynamics of the system (3). We present the following theorem:

**Theorem 3** Let  $N = S + V + E + A + I + R$  and

$$\Gamma = \left\{ (S, V, E, A, I, R) \in \mathbb{R}_+^6 \mid 0 \leq S + V + E + A + I + R = N \leq \frac{\Pi}{\mu} \right\}.$$

It can be demonstrated that the closed set  $\Gamma$  is positively invariant under the dynamics of the system (3).

*Proof* We can confirm that  $N$  is the total population of the model under consideration. By computing fractional derivative at  $\zeta \in (0, 1]$ , we get

$$\begin{aligned} \mathbb{ABC} D_t^\zeta N(t) &= \mathbb{ABC} D_t^\zeta S(t) + \mathbb{ABC} D_t^\zeta V(t) + \mathbb{ABC} D_t^\zeta E(t) + \mathbb{ABC} D_t^\zeta A(t) + \mathbb{ABC} D_t^\zeta I(t) + \mathbb{ABC} D_t^\zeta R(t) \\ &= \Pi - \mu(S + V + E + A + I + R) - dI. \end{aligned} \tag{22}$$

We obtain the following by using the Laplace transform on Eq. (22) both sides:

$$\begin{aligned} \mathcal{L}[\mathbb{ABC} D_t^\zeta(N(t))] &= \mathcal{L}[\Pi - \mu N - dI] \leq \mathcal{L}[\Pi - \mu N], \\ \frac{\mathbb{ABC}(\zeta) s^\zeta N(s)}{s^\zeta(1-\zeta) + \zeta} + \mu N(s) &\leq \frac{\Pi}{s} + \frac{\mathbb{ABC}(\zeta) s^{\zeta-1} N(0)}{s^\zeta(1-\zeta) + \zeta}, \end{aligned} \tag{23}$$

where  $N(s)$  will represent the Laplace transform of  $[N(t)](s)$  and  $N(0)$  is the initial condition. Write (23) in term of  $N(s)$ , we have

$$N(s) \leq \frac{\Pi s^{\zeta-(\zeta+1)}[s^{\zeta}(1-\zeta) + \zeta] + \mathbb{A}\mathbb{B}\mathbb{C}(\zeta)s^{\zeta-1}N(0)}{\mathbb{A}\mathbb{B}\mathbb{C}(\zeta)s^{\zeta} + \mu[s^{\zeta}(1-\zeta) + \zeta]},$$

Therefore,

$$\begin{aligned} N(s) &\leq \frac{\Pi s^{\zeta-(\zeta+1)}[s^{\zeta}(1-\zeta) + \zeta]}{[\mathbb{A}\mathbb{B}\mathbb{C}(\zeta) + (1-\zeta)\mu]s^{\zeta} + \mu\zeta} + \frac{\mathbb{A}\mathbb{B}\mathbb{C}(\zeta)s^{\zeta-1}N(0)}{[\mathbb{A}\mathbb{B}\mathbb{C}(\zeta) + (1-\zeta)\mu]s^{\zeta} + \mu\zeta}, \\ &= \left( \frac{\Pi(1-\zeta)}{[\mathbb{A}\mathbb{B}\mathbb{C}(\zeta) + (1-\zeta)\mu]} \right) \frac{s^{\zeta-1}}{s^{\zeta} + \frac{\mu\zeta}{\mathbb{A}\mathbb{B}\mathbb{C}(\zeta) + (1-\zeta)\mu}} \\ &+ \left( \frac{\Pi\zeta}{\mathbb{A}\mathbb{B}\mathbb{C}(\zeta) + (1-\zeta)\mu} \right) \frac{s^{\zeta-(\zeta+1)}}{s^{\zeta} + \frac{\mu\zeta}{\mathbb{A}\mathbb{B}\mathbb{C}(\zeta) + (1-\zeta)\mu}} \\ &+ \left( \frac{\mathbb{A}\mathbb{B}\mathbb{C}(\zeta)N(0)}{\mathbb{A}\mathbb{B}\mathbb{C}(\zeta) + \mu(1-\zeta)} \right) \frac{s^{\zeta-1}}{s^{\zeta} + \frac{\mu\zeta}{\mathbb{A}\mathbb{B}\mathbb{C}(\zeta) + \mu(1-\zeta)}}, \end{aligned}$$

Exerting inverse Laplace transform on both sides, we obtained the following inequalities

$$\begin{aligned} N(s) &\leq \left( \frac{\Pi(1-\zeta)}{\mathbb{A}\mathbb{B}\mathbb{C}(\zeta) + (1-\zeta)\mu} + \frac{\mathbb{A}\mathbb{B}\mathbb{C}(\zeta)N(0)}{\mathbb{A}\mathbb{B}\mathbb{C}(\zeta) + (1-\zeta)\mu} \right) E_{\zeta,1} \left( \frac{-\zeta\mu t^{\zeta}}{\mathbb{A}\mathbb{B}\mathbb{C}(\zeta) + (1-\zeta)\mu} \right) \\ &+ \left( \frac{\Pi\zeta t^{\zeta}}{\mathbb{A}\mathbb{B}\mathbb{C}(\zeta) + (1-\zeta)\mu} \right) E_{\zeta,\zeta+1} \left( \frac{-\zeta\mu t^{\zeta}}{\mathbb{A}\mathbb{B}\mathbb{C}(\zeta) + (1-\zeta)\mu} \right), \end{aligned} \tag{24}$$

MLF with two parameter  $p > 0, q > 0$  is interpreted as

$$E_{p,q}(Y) = \sum_{j=0}^{\infty} \frac{Y^j}{pj + q}$$

Laplace transform of this function is,

$$\mathcal{L}[t^{q-1}E_{p,q}(\pm\nu t^p)] = \frac{s^{p-q}}{s^p \mp \nu}$$

Given that  $s > |\nu|^{\frac{1}{p}}$ . MLF gratify<sup>2</sup>

$$E_{p,q}(Y) = \frac{1}{Y} \left[ E_{p,q-p}(Y) - \frac{1}{\Gamma(q-p)} \right] \tag{25}$$

The MLF has asymptotic behavior, which is given as follows by<sup>31</sup>,

$$E_{q,q+1}(Y) \approx \sum_{j=1}^i \frac{Y^{-j}}{q + (q+1)j} + \mathcal{O}(|Y|^{-1-i}), |Y| \rightarrow \infty, \frac{q\pi}{2} < |\arg Y| \leq \pi. \tag{26}$$

Follows from Eqs. (24) to (25) and (26), one can see the result,  $N(t) \leq \frac{\Pi}{\mu}$  as  $t \rightarrow \infty$ . Consequently,  $\Gamma$  is interpreted as positively invariant in the region concerning (3). □

### Solution non-negativity

We now demonstrate that the solution to model (3) remains non-negative for all variables, provided that the ICs are non-negative. We provide the following result:

**Theorem 4** *The solution of associated with the system (3) will always remain non-negative, provided that the ICs are non-negative.*

*Proof* Let's begin with the first equation of the system (3), given by:

$$\begin{aligned} {}_0^{\mathbb{A}\mathbb{B}\mathbb{C}}D_t^{\zeta}S(t) &= \Pi - \frac{(a_1I + a_2A)S}{N} - (\mu + \omega)S + \kappa R + \theta V \\ &\geq - \left( \frac{(a_1I + a_2A)}{N} + (\mu + \omega) \right) S \end{aligned}$$

According to Theorem 3, all populations are confined within bounds, and therefore, we have:

$$\max \left\{ S, V, E, A, I, R \right\} \leq M, \quad M > 0. \tag{27}$$

So, we get

$${}_{0}^{\text{ABC}} D_t^\zeta S(t) \geq -c_1 S$$

where  $c_1 = \frac{(a_1 I + a_2 A)}{N} + (\mu + \omega)$ . The application of Laplace transform and its inverse, as described previously, we get the below result:

$$S(t) = \frac{{}_{\text{ABC}}(\zeta) S(0) s^{\zeta-1}}{{}_{\text{ABC}}(\zeta) + c_1(1 - \zeta)} E_{\zeta,1} \left( \frac{-\zeta t^\zeta c_1}{{}_{\text{ABC}}(\zeta) + c_1(1 - \zeta)} \right). \tag{28}$$

Utilizing the characteristics of MLF, the terms on the right-hand side of the bounding Eq. (28) guarantee that  $S \geq 0$  for all  $t \geq 0$ . In the same way, we are able to confirm that  $V \geq 0, E \geq 0, A \geq 0, I \geq 0$ , and  $R \geq 0$ . This completes the proof.  $\square$

The potential equilibrium points of model (3) will be examined in the following subsection:

### Disease Free Equilibrium (DFE)

We represent the DFE of the system (3) by  $E_0$  which is given by,

$$E_0 = (S_0, V_0, E_0, A_0, I_0, R_0) = \left( \frac{\Pi(\theta + \mu)}{\mu(\theta + \mu + \omega)}, \frac{\Pi\omega}{\mu(\theta + \mu + \omega)}, 0, 0, 0, 0 \right).$$

### Basic reproduction number ( $\mathcal{R}_0$ )

The basic reproduction number with the vaccine  $\mathcal{R}_v$  is provided in<sup>28</sup>, specifically,

$$\mathcal{R}_v = \frac{(\theta + \mu + \omega(1 - \psi))}{(\mu + \delta)(\theta + \mu + \omega)} \left( \frac{a_1 \delta(1 - q)}{(d + \mu + \rho)} + \frac{a_2 \delta q}{(\mu + \rho_1)} \right).$$

The value of  $\mathcal{R}_0$  stands for the mean number of person to person transmission in a community. When  $\psi = 1$  and  $\omega = \theta = 0$ ,  $\mathcal{R}_v$  simplifies to the number of generations in a population at which the transmission of the social infection is maintained ( $\mathcal{R}_0$ ):

$$\mathcal{R}_0 = \frac{1}{(\mu + \delta)} \left( \frac{a_1 \delta(1 - q)}{(d + \mu + \rho)} + \frac{a_2 \delta q}{(\mu + \rho_1)} \right).$$

### Endemic steady state point

We have the expression for the endemic equilibrium (EE) for the system (3) is shown by  $E_1$  and obtained as follows:

$$E_1 = (S_*, V_*, E_*, A_*, I_*, R_*).$$

where

$$\begin{cases} S_* = \frac{\theta V_* + \Pi + \kappa R_*}{\beta_* + \mu + \omega}, & V_* = \frac{\omega S_*}{\mu + \theta + (1 - \psi)\beta_*}, \\ E_* = \frac{\beta_*(S_* + (1 - \psi)V_*)}{\mu + \delta}, & A_* = \frac{q\delta E_*}{\rho_1 + \mu}, \\ I_* = \frac{\delta(1 - q)E_*}{d + \mu + \rho}, & R_* = \frac{\rho I_* + \rho_1 A_*}{\kappa + \mu}. \end{cases} \tag{29}$$

When the expression given in (29) are substituted in  $\beta_* = \frac{\beta_1 I_* + \beta_2 A_*}{S_* + V_* + E_* + A_* + I_* + R_*}$ , we obtain a quadratic equation in  $\beta_*$  and it is given below:

$$b_1 \beta_*^2 + b_2 \beta_* + b_3 = 0. \tag{30}$$

where

$$\begin{cases} b_1 = (1 - \psi)(\mu + \rho_1)((\kappa + \mu)(\mu + d + \delta(1 - q) + \rho) + \delta(1 - q)\rho) + \\ \delta q(1 - \psi)(d + \mu + \rho)(\rho_1 + \kappa + \mu), \\ b_2 = (1 - \psi)(d + \mu + \rho)(\kappa + \mu)[(\rho_1 + \mu)(\delta + \mu + \omega) + \delta q(\omega - a_2)] + \delta \rho_1 q \omega + \\ \delta(1 - q)(1 - \psi)(\rho_1 + \mu)[(\omega - a_1)(\kappa + \mu) + \rho \omega] + (\theta + \mu)(d + \mu + \rho) \\ \times ((\kappa + \mu)(\rho_1 + \mu + \delta q) + \delta \rho_1 q) + \delta(1 - q)(\rho_1 + \mu)(\theta + \mu)(\kappa + \mu + \rho), \\ b_3 = (\kappa + \mu)(\mu + d + \rho)(\mu + \rho_1)(\delta + \mu)(\mu + \omega + \theta)(\theta + \mu + (1 - \psi)\omega)(1 - \mathcal{R}_v). \end{cases}$$

For more details about this, we refer the reader to see<sup>28</sup>. Further, the work in<sup>28</sup>, has explained in details the stability of DFE and EE, so we omit it here, see<sup>28</sup>.

### Parameter estimation

This section outlines the estimation process for the model parameters based on real COVID-19 data in Pakistan. The cumulative confirmed cases from 13 May 2022 to 30 September 2022 were obtained from a reliable online source<sup>33,34</sup>. All simulations were conducted using a daily time scale.

A nonlinear least-squares curve fitting technique was applied to estimate the model parameters by fitting the model to the observed cumulative data. The model considered for parameter fitting excluded vaccination, focusing on the natural transmission dynamics of the disease. Some of the parameters involved in the model such as the natural birth rate  $\Pi = 9330$  and the natural death rate  $\mu = \frac{1}{67.7 \times 365}$  were computed directly from demographic data. The remaining parameters were estimated by fitting the model output to the reported case data.

The total population of Pakistan in 2022 was considered as  $N(0) = 230,557,367$ <sup>35</sup>. The initial values for the model compartments were given by:  $S(0) = 230,255,033$ ,  $E(0) = 3 \times 10^5$ ,  $A(0) = 2 \times 10^3$ ,  $I(0) = 334$  (the reported symptomatic cases on 13 May 2022), and  $R(0) = 0$ . There is no specific information regarding the exposed and asymptomatic are assumed as a best fit in model fitting.

After fitting, the estimated parameter values were obtained and is given in Table 1. Using these fitted parameters, the basic reproduction number was computed to be approximately  $\mathcal{R}_0 \approx 1.2591$ , indicating the potential for sustained transmission in the absence of interventions.

The data fitting results are shown in Fig. 1(a), which demonstrates a strong agreement between the model and observed case data, validating the estimated parameters. Figure 1 (b) represents the corresponding residual of the data fitting.

In the next phase of the study, we introduce vaccination into the model to assess its impact on controlling the outbreak. In this context, the parameter  $\omega$  represents the vaccination rate of susceptible individuals and is set to  $\omega = 0.001$ . The vaccine efficacy is modeled by  $\psi = 0.6$ , and waning immunity following vaccination is captured by the parameter  $\theta = 0.01$ . These values account for imperfect vaccine protection and the gradual loss of immunity over time, which are critical factors in the evaluation of long-term disease control strategies.

### Sensitivity analysis

In order to analyze the interactions of the different parameters of our model, we use Latin Hypercube Sampling (LHS), a method for generating sets of parameter sets, such that each dimension is sampled across the entire domain with probability density proportional to the given density for each variable<sup>3,36,37</sup>. Meanwhile, to assess the degree of variability in the model parameters, LHS is combined PRCCs.

We use the discretization approximation and assume that there are uncertain parameters that have a chance variable distributed uniformly within  $\pm 30\%$  of a baseline value. Latin Hypercube Sampling was performed for these distributions with 1000 samples being randomly created. Partial Rank Correlation Coefficients (PRCCs) were calculated for each of the following parameters:  $(\mu, a_1, a_2, \omega, \theta, \psi, \delta, q, \rho_1, \rho, d)$  in relation to the outcome variable, the basic reproduction number  $\mathcal{R}_v$ . The sign of the PRCC indicates whether variations in the input parameters have a positive or negative impact on the output variable<sup>38,39</sup>.

Parameter	Description	Value	Source
$\Pi$	Recruitment rate into susceptible population	230557367 $\mu$	Estimated
$a_1$	Asymptomatic infection rate	0.8983	Fitted
$a_2$	Symptomatic infection rate	0.3827	Fitted
$\mu$	Natural mortality rate	$1/(67.7 \times 365)$	<sup>32</sup>
$\kappa$	Rate of loss of immunity	0.3129	Fitted
$\delta$	Exposed duration	0.9982	Fitted
$q$	Fraction of exposed people	0.9931	Fitted
$\rho_1$	Asymptomatic recovery rate	0.3028	Fitted
$\rho$	Symptomatic recovery rate	0.7926	Fitted
$d$	Symptomatic case fatality rate	0.6784	Fitted

**Table 1.** Description of the parameters obtained from the fitting process (3).

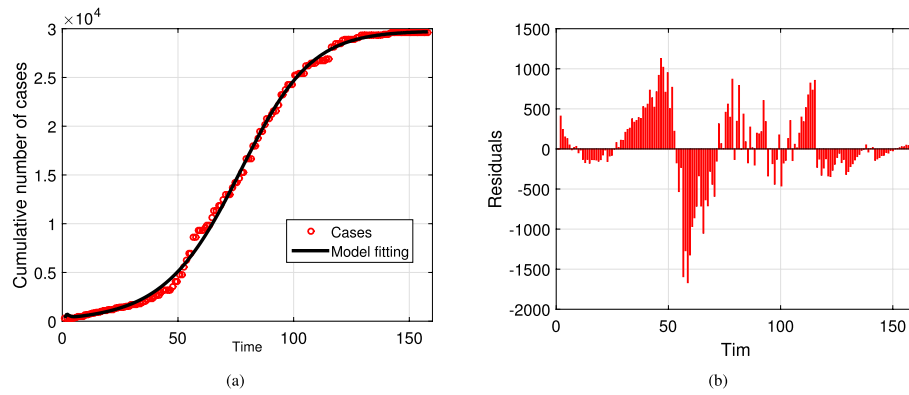


**Fig. 1.** The graph represents the data fitting of the model (3) for  $\zeta = 1$ , and their corresponding residuals. Sub-figures (a) and (b) respectively represents the model versus data fitting and their corresponding residuals.

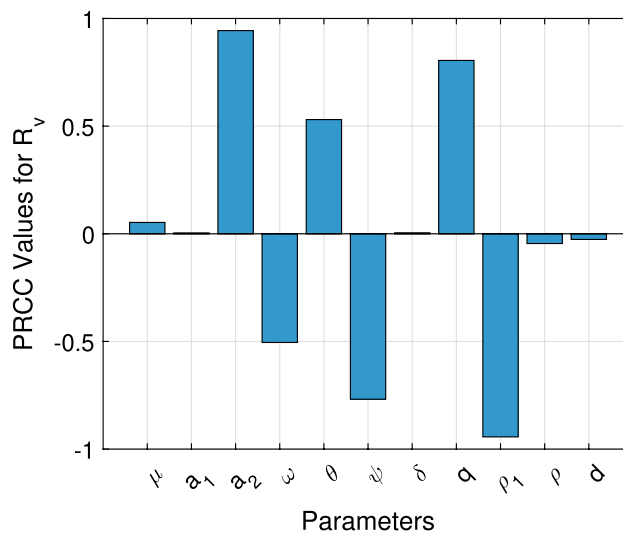


**Fig. 2.** Sensitivity analysis showing PRCC results that demonstrate the dependence of  $\mathcal{R}_v$  on the model parameters.

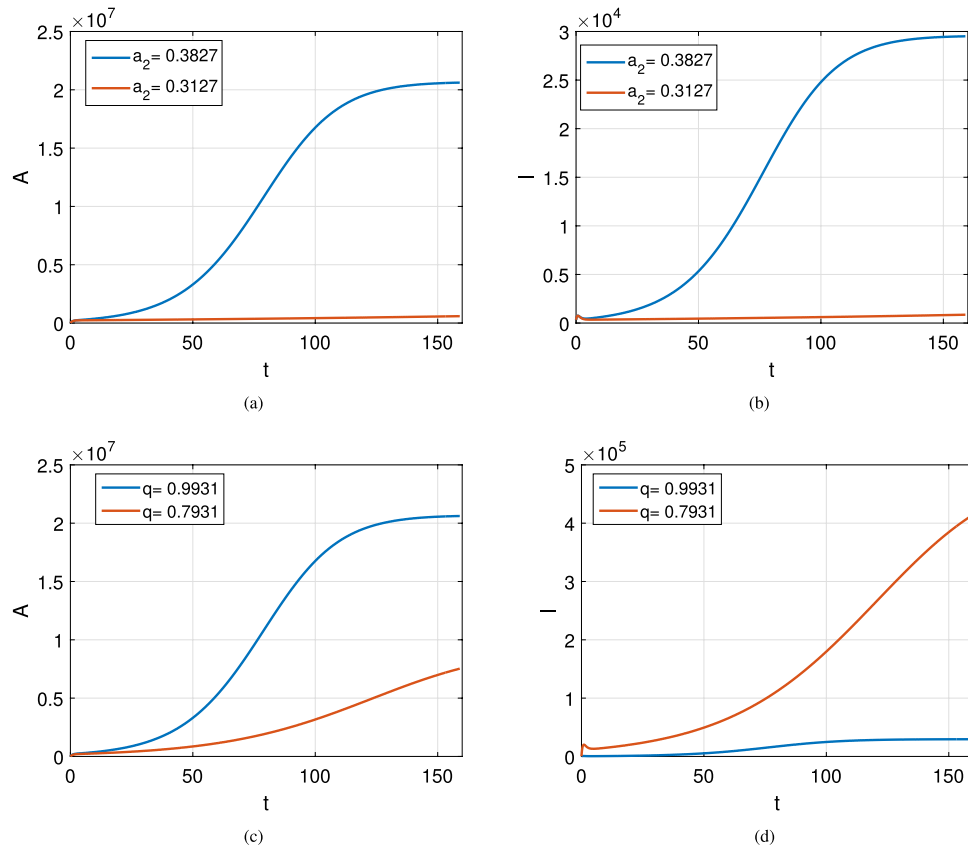
Parameters with PRCC values greater than 0.4 (in absolute value) are considered to have a strong influence, with a negative PRCC indicating an inverse relationship<sup>38,39</sup>. A moderate correlation is defined for parameters with  $0.2 < |PRCC| < 0.4$ , while weaker correlations are observed when  $|PRCC| \leq 0.2$ <sup>40</sup>.

Figure 2 highlight that the parameters  $(a_2, \theta, q, \omega, \psi, \rho_1)$  exhibits the most significant impact on the outcome function, specifically the reproduction number  $\mathcal{R}_v$ . Conversely, the parameters  $(\mu, a_1, \delta, \rho, d)$  demonstrate a moderate impact on the basic reproduction number. We see in Fig. 3 (a) to (b) that decreasing  $a_2$  reducing the basic reproduction number from 1.2591 to 1.0296 which shows a strong impact in absence of vaccination, and so the number of cases in asymptomatic and symptomatic classes are decreased well. Similarly, in Fig. 3 (c) to (d), when reducing  $q$ , the asymptomatic cases decreases while in (d) the symptomatic cases increases which shows an impact for the basic reproduction number reduce it to 1.1285. The key parameters that contribute to increasing the reproduction number  $\mathcal{R}_v$  are the transmission rate  $a_2$ . On the contrary, the parameters that lead to a decrease in  $\mathcal{R}_v$  include the proportion of natural death rate  $\mu$ .

Epidemiology often faces challenges in predicting the daily infection rate, as it tends to fluctuate based on the prevailing circumstances. This variability can be incorporated by applying a stochastic process. By accounting for environmental white noise, the model in (3) is transferred into a stochastic system, incorporating the derivative of Brownian motion, through the introduction of nonlinear perturbations in each of the model<sup>40</sup>. A detailed explanation for such derivation and of how the model is transformed into its stochastic version can be found in<sup>41,42</sup>.

### Stochastic fractional model using ABC derivative

In real-world disease dynamics, not everything follows a fixed pattern random events, unpredictable behavior, and inconsistencies in data reporting often play a major role. A purely deterministic model assumes perfect knowledge and uniform behavior, which isn't always realistic. That's why incorporating randomness, or



**Fig. 3.** The impact of  $a_2 = 0.3827, 0.3127$  and  $q = 0.9931, 0.7931$  on the asymptomatic and symptomatic individuals, see Sub-Fig. 3 (a) and (c), and symptomatic compartments, see Sub-Fig. 3(b), and (d).

stochasticity, becomes essential. By transitioning to a stochastic fractional model, especially one based on the Atangana–Baleanu–Caputo (ABC) derivative, we can better reflect the unpredictable nature of disease transmission. This approach adds a layer of realism, accounting for the chance-driven variations that a deterministic model might miss. The stochastic fractional model in ABC sense is given below:

$$\begin{cases} {}_0^{\text{ABC}}D_t^\zeta S(t) = \Pi - \frac{(a_1 I + a_2 A)S}{N} - (\mu + \omega)S + \kappa R + \theta V + \nu_1 H_1(t, S)\dot{W}_0(t), \\ {}_0^{\text{ABC}}D_t^\zeta V(t) = \omega S - (1 - \psi)\frac{(a_1 I + a_2 A)V}{N} - (\theta + \mu)V + \nu_2 H_2(t, V)\dot{W}_1(t), \\ {}_0^{\text{ABC}}D_t^\zeta E(t) = \frac{(a_1 I + a_2 A)S}{N} + (1 - \psi)\frac{(a_1 I + a_2 A)V}{N} - (\delta + \mu)E + \nu_3 H_3(t, E)\dot{W}_2(t), \\ {}_0^{\text{ABC}}D_t^\zeta A(t) = \delta q E - (\mu + \rho_1)A + \nu_4 H_4(t, A)\dot{W}_3(t), \\ {}_0^{\text{ABC}}D_t^\zeta I(t) = (1 - q)\delta E - (\mu + d + \rho)I + \nu_5 H_5(t, I)\dot{W}_4(t), \\ {}_0^{\text{ABC}}D_t^\zeta R(t) = \rho I + \rho_1 A - (\kappa + \mu)R + \nu_6 H_6(t, R)\dot{W}_5(t). \end{cases} \quad (31)$$

$$S(0) = S_0 > 0, \quad V(0) = V_0 \geq 0, \quad E(0) = E_0 \geq 0, \quad A(0) = A_0 \geq 0, \quad I(0) = I_0 \geq 0, \quad R(0) = R_0 \geq 0.$$

where  $W_0(\cdot), W_1(\cdot), W_2(\cdot), W_3(\cdot), W_4(\cdot), W_5(\cdot)$  depicts the standard Brownian motion and  $H_1, H_2, H_3, H_4, H_5, H_6$  represents the stochastic constants, and  $\nu_i$ , for  $i = 1, \dots, 6$  are noise intensity parameters.

**Existence and Uniqueness (EU)**

Here we examine the EU of the solution to system (31) in the presence of stochastic components.

$$\begin{cases} {}_0^{\text{ABC}}D_t^\zeta S(t) - H_{11}(S, t) = \nu_1 H_1(t, S)\dot{W}_0(t), \\ {}_0^{\text{ABC}}D_t^\zeta V(t) - H_{12}(V, t) = \nu_2 H_2(t, V)\dot{W}_1(t), \\ {}_0^{\text{ABC}}D_t^\zeta E(t) - H_{13}(A, t) = \nu_3 H_3(t, E)\dot{W}_2(t), \\ {}_0^{\text{ABC}}D_t^\zeta A(t) - H_{14}(E, t) = \nu_4 H_4(t, A)\dot{W}_3(t), \\ {}_0^{\text{ABC}}D_t^\zeta I(t) - H_{15}(I, t) = \nu_5 H_5(t, I)\dot{W}_4(t), \\ {}_0^{\text{ABC}}D_t^\zeta R(t) - H_{16}(R, t) = \nu_6 H_6(t, R)\dot{W}_5(t). \end{cases} \quad (32)$$

where

$$\begin{cases} H_{11}(S, t) = \Pi - \frac{(a_1 I + a_2 A)S}{N} - (\mu + \omega)S + \kappa R + \theta V, \\ H_{12}(V, t) = \omega S - (1 - \psi) \frac{(a_1 I + a_2 A)V}{N} - (\theta + \mu)V, \\ H_{13}(A, t) = \frac{(a_1 I + a_2 A)S}{N} + (1 - \psi) \frac{(a_1 I + a_2 A)V}{N} - (\delta + \mu)E, \\ H_{14}(E, t) = \delta q E - (\mu + \rho_1)A, \\ H_{15}(I, t) = (1 - q)\delta E - (\mu + d + \rho)I, \\ H_{16}(R, t) = \rho I + \rho_1 A - (\kappa + \mu)R. \end{cases} \tag{33}$$

The following conditions are proved,  $|H_{1i}(t, Y_i)|^2$ ,

$$|H_i(t, Y_i)|^2 < K_i(1 + |Y_i|^2), \quad \forall t \in [0, T],$$

and  $|H_{1i}(t, Y_i^1) - H_{1i}(t, Y_i^2)|^2$ ,

$$|H_i(t, Y_i^1) - H_i(t, Y_i^2)|^2 < \bar{K}_i(|Y_i^1 - Y_i^2|^2), \quad \forall t \in [0, T], \quad \text{for } i = 1, 2, \dots, 6.$$

, and  $Y_i = S, V, A, E, I, R$ .

$$\begin{aligned} |H_{11}(S, t)|^2 &= \left| \Pi - \frac{(a_1 I + a_2 A)S}{N} - (\mu + \omega)S + \kappa R + \theta V \right|^2, \\ &\leq 3 \left( \pi^2 + \frac{|S|^2}{N^2} (a_1^2 |I|^2 + a_2^2 |A|^2) + (\mu + \omega)^2 |S|^2 + \theta^2 |V|^2 + \kappa^2 |R|^2 \right), \\ &\leq 3 \left( \pi^2 + \frac{|S|^2}{N^2} \left( a_1^2 \sup_{0 \leq t \leq T} |I|^2 + a_2^2 \sup_{0 \leq t \leq T} |A|^2 \right) + (\mu + \omega)^2 |S|^2 + \theta^2 \sup_{0 \leq t \leq T} |V|^2 + \kappa^2 \sup_{0 \leq t \leq T} |R|^2 \right), \\ &\leq 3 \left( \pi^2 + \frac{|S|^2}{N^2} \left( a_1^2 \|I\|_\infty + a_2^2 \|A\|_\infty \right) + (\mu + \omega)^2 |S|^2 + \theta^2 \|V\|_\infty + \kappa^2 \|R\|_\infty \right), \tag{34} \\ &\leq 3 \left( \left( \pi^2 + \theta^2 \|V\|_\infty + \kappa^2 \|R\|_\infty \right) + \left( \frac{1}{N^2} \left( a_1^2 \|I\|_\infty + a_2^2 \|A\|_\infty \right) + (\mu + \omega)^2 \right) |S|^2 \right), \\ &\leq 3 \left( \pi^2 + \theta^2 \|V\|_\infty + \kappa^2 \|R\|_\infty \right) \left( 1 + \frac{\frac{1}{N^2} \left( a_1^2 \|I\|_\infty + a_2^2 \|A\|_\infty \right) + (\mu + \omega)^2}{K_1/3} |S|^2 \right), \\ &\leq K_1(1 + |S|^2). \end{aligned}$$

where  $K_1 = 3 \left( \pi^2 + \theta^2 \|V\|_\infty + \kappa^2 \|R\|_\infty \right)$  and  $\frac{\frac{1}{N^2} \left( a_1^2 \|I\|_\infty + a_2^2 \|A\|_\infty \right) + (\mu + \omega)^2}{K_1/3} < 1$ .

$$\begin{aligned}
|H_{12}(V, t)|^2 &= \left| \omega S - (1 - \psi) \frac{(a_1 I + a_2 A)V}{N} - (\theta + \mu)V \right|^2, \\
&\leq 3 \left( \omega^2 |S|^2 + (1 - \psi)^2 \frac{1}{N^2} \left( a_1^2 |I|^2 + a_2^2 |A|^2 \right) |V|^2 + (\theta + \mu)^2 |V|^2 \right), \\
&\leq 3 \left( \omega^2 \sup_{0 \leq t \leq T} |S|^2 + \frac{(1 + \psi)^2}{N^2} \left( a_1^2 \sup_{0 \leq t \leq T} |I|^2 + a_2^2 \sup_{0 \leq t \leq T} |A|^2 \right) |V|^2 + (\theta + \mu)^2 |V|^2 \right), \\
&\leq 3 \left( \omega^2 \|S^2\|_\infty + \frac{(1 + \psi)^2}{N^2} \left( a_1^2 \|I^2\|_\infty + a_2^2 \|A^2\|_\infty \right) |V|^2 + (\theta + \mu)^2 |V|^2 \right), \\
&\leq 3\omega^2 \|S^2\|_\infty \left( 1 + \frac{\frac{(1 + \psi)^2}{N^2} \left( a_1^2 \|I^2\|_\infty + a_2^2 \|A^2\|_\infty \right) + (\theta + \mu)^2}{K_2/3} |V|^2 \right), \\
&\leq K_2(1 + |V|^2).
\end{aligned} \tag{35}$$

where  $K_2 = 3\omega^2 \|S^2\|_\infty$  and  $\frac{\frac{(1 + \psi)^2}{N^2} \left( a_1^2 \|I^2\|_\infty + a_2^2 \|A^2\|_\infty \right) + (\theta + \mu)^2}{K_2/3} < 1$ .

$$\begin{aligned}
|H_{13}(E, t)|^2 &= \left| \frac{(a_1 I + a_2 A)S}{N} + (1 - \psi) \frac{(a_1 I + a_2 A)V}{N} - (\delta + \mu)E \right|^2, \\
&\leq \frac{3}{N^2} \left( |S|^2 + (1 - \psi)^2 |V|^2 \right) \left( a_1^2 |I|^2 + a_2^2 |A|^2 \right) + (\delta + \mu)^2 |E|^2, \\
&\leq \frac{3}{N^2} \left( \sup_{0 \leq t \leq T} |S|^2 + (1 + \psi)^2 \sup_{0 \leq t \leq T} |V|^2 \right) \left( a_1^2 \sup_{0 \leq t \leq T} |I|^2 + a_2^2 \sup_{0 \leq t \leq T} |A|^2 \right) + (\delta + \mu)^2 |E|^2, \\
&\leq \frac{3}{N^2} \left( \|S^2\|_\infty + (1 + \psi)^2 \|V^2\|_\infty \right) \left( a_1^2 \|I^2\|_\infty + a_2^2 \|A^2\|_\infty \right) + (\delta + \mu)^2 |E|^2, \\
&\leq 3 \frac{1}{N^2} \left( \|S^2\|_\infty + (1 + \psi)^2 \|V^2\|_\infty \right) \left( a_1^2 \|I^2\|_\infty + a_2^2 \|A^2\|_\infty \right) \times \\
&\quad \left( 1 + \frac{(\delta + \mu)^2}{\frac{1}{N^2} \left( \|S^2\|_\infty + (1 + \psi)^2 \|V^2\|_\infty \right) \left( a_1^2 \|I^2\|_\infty + a_2^2 \|A^2\|_\infty \right)} |E|^2 \right), \\
&\leq K_3 \left( 1 + \frac{(\delta + \mu)^2}{K_3/3} |E|^2 \right), \\
&\leq K_3(1 + |E|^2).
\end{aligned} \tag{36}$$

where  $K_3 = 3 \frac{1}{N^2} \left( \|S^2\|_\infty + (1 + \psi)^2 \|V^2\|_\infty \right) \left( a_1^2 \|I^2\|_\infty + a_2^2 \|A^2\|_\infty \right)$  and  $\frac{(\delta + \mu)^2}{K_3/3} < 1$ .

$$\begin{aligned}
 |H_{14}(A, t)|^2 &= \left| \delta q E - (\mu + \rho_1) A \right|^2, \\
 &\leq 3 \left( \delta^2 q^2 \sup_{0 \leq t \leq T} |E|^2 + (\rho_1 + \mu)^2 |A|^2 \right), \\
 &\leq 3 \left( \delta^2 q^2 \|E^2\|_\infty + (\rho_1 + \mu)^2 |A|^2 \right), \\
 &\leq 3 \delta^2 q^2 \|E^2\|_\infty \left( 1 + \frac{(\rho_1 + \mu)^2}{K_4/3} |A|^2 \right), \\
 &\leq K_4 (1 + |A|^2),
 \end{aligned}
 \tag{37}$$

where  $K_4 = 3\delta^2 q^2 \|E^2\|_\infty$  and  $\frac{(\rho_1 + \mu)^2}{K_4/3} < 1$ .

$$\begin{aligned}
 |H_{15}(I, t)|^2 &= \left| (1 - q) \delta E - (\mu + d + \rho) I \right|^2, \\
 &\leq 3 \left( \delta^2 (1 + q)^2 |E|^2 + (\mu + d + \rho)^2 |I|^2 \right), \\
 &\leq 3 \left( \delta^2 (1 + q)^2 \sup_{0 \leq t \leq T} |E|^2 + (\mu + d + \rho)^2 |I|^2 \right), \\
 &\leq 3 \left( \delta^2 (1 + q)^2 \|E^2\|_\infty + (\mu + d + \rho)^2 |I|^2 \right), \\
 &\leq 3 \delta^2 (1 + q)^2 \|E^2\|_\infty \left( 1 + \frac{(\rho + \mu + d)^2}{K_5/3} |I|^2 \right), \\
 &\leq K_5 (1 + |I|^2),
 \end{aligned}
 \tag{38}$$

where  $K_5 = 3\delta^2 (1 + q)^2 \|E^2\|_\infty$  and  $\frac{(\rho + \mu + d)^2}{K_5/3} < 1$ .

$$\begin{aligned}
 |H_{15}(R, t)|^2 &= \left| \rho I + \rho_1 A - (\kappa + \mu) R \right|^2, \\
 &\leq 3 \left( \rho^2 |I|^2 + (\kappa + \mu)^2 |R|^2 \right), \\
 &\leq 3 \left( \rho^2 \sup_{0 \leq t \leq T} |I|^2 + (\kappa + \mu)^2 |R|^2 \right), \\
 &\leq 3 \left( \rho^2 \|I^2\|_\infty + (\kappa + \mu)^2 |R|^2 \right), \\
 &\leq 3 \rho^2 \|I^2\|_\infty \left( 1 + \frac{(\kappa + \mu)^2}{K_6/3} |R|^2 \right), \\
 &\leq K_6 (1 + |R|^2).
 \end{aligned}
 \tag{39}$$

where  $K_6 = 3\rho^2 \|I^2\|_\infty$  and  $\frac{(\kappa+\mu)^2}{K_6/3} < 1$ . We get the following, for every  $t \in [0, T]$ :

$$\begin{cases} |H_1(t, S)|^2 = \nu_1^2 |S|^2 \leq \nu_1^2 (1 + |S|^2), & |H_2(t, V)|^2 = \nu_2^2 |V|^2 \leq \nu_2^2 (1 + |V|^2), \\ |H_3(t, E)|^2 = \nu_3^2 |E|^2 \leq \nu_3^2 (1 + |E|^2), & |H_4(t, A)|^2 = \nu_4^2 |A|^2 \leq \nu_4^2 (1 + |A|^2), \\ |H_5(t, I)|^2 = \nu_5^2 |I|^2 \leq \nu_5^2 (1 + |I|^2), & |H_6(t, R)|^2 = \nu_6^2 |R|^2 \leq \nu_6^2 (1 + |R|^2). \end{cases} \tag{40}$$

We verifying the other condition given by,

$$\begin{cases} |H_{11}(t, S) - H_{11}(t, S_1)|^2 = |\Pi - \frac{(a_1 I + a_2 A)S}{N} - (\mu + \omega)S + \kappa R + \theta V - \\ \Pi + \frac{(a_1 I + a_2 A)S_1}{N} + (\mu + \omega)S_1 - \kappa R - \theta V|^2, \\ = | - \frac{(a_1 I + a_2 A)(S - S_1)}{N} - (\mu + \omega)(S - S_1)|^2, \\ \leq 4 \left( \frac{(a_1^2 |I|^2 + a_2^2 |A|^2) |S - S_1|^2}{N^2} + (\mu + \omega)^2 |S - S_1|^2 \right) \\ \leq 4 \left( \frac{(a_1^2 \|I^2\|_\infty + a_2^2 \|A^2\|_\infty)}{N^2} + (\mu + \omega)^2 \right) |S - S_1|^2 \\ \leq \bar{K}_1 |S - S_1|^2. \end{cases} \tag{41}$$

$$\begin{cases} |H_{12}(t, V) - H_{12}(t, V_1)|^2 = |\omega S - (1 - \psi) \frac{(a_1 I + a_2 A)V}{N} - (\theta + \mu)V - \\ \omega S + (1 - \psi) \frac{(a_1 I + a_2 A)V_1}{N} + (\theta + \mu)V_1|^2, \\ = | - (1 - \psi) \frac{(a_1 I + a_2 A)(V - V_1)}{N} - (\theta + \mu)(V - V_1)|^2, \\ \leq 4 \left( (1 + \psi)^2 \frac{(a_1^2 |I|^2 + a_2^2 |A|^2) |V - V_1|^2}{N^2} + (\theta + \mu)^2 |V - V_1|^2 \right) \\ \leq 4 \left( (1 + \psi)^2 \frac{(a_1^2 \|I^2\|_\infty + a_2^2 \|A^2\|_\infty)}{N^2} + (\mu + \theta)^2 \right) |V - V_1|^2 \\ \leq \bar{K}_2 |V - V_1|^2. \end{cases} \tag{42}$$

$$\begin{cases} |H_{13}(t, E) - H_{13}(t, E_1)|^2 = | \frac{(a_1 I + a_2 A)S}{N} + (1 - \psi) \frac{(a_1 I + a_2 A)V}{N} - (\delta + \mu)E - \\ \frac{(a_1 I + a_2 A)S}{N} - (1 - \psi) \frac{(a_1 I + a_2 A)V}{N} + (\delta + \mu)E_1|^2, \\ = | - (\delta + \mu)(E - E_1)|^2, \\ \leq 4(\delta + \mu)^2 |E - E_1|^2 \\ \leq \bar{K}_3 |E - E_1|^2. \end{cases} \tag{43}$$

$$\begin{cases} |H_{14}(t, A) - H_{14}(t, A_1)|^2 = |\delta q E - (\mu + \rho_1)A - \delta q E + (\mu + \rho_1)A_1|^2, \\ = | - (\mu + \rho_1)(A - A_1)|^2, \\ \leq 4(\mu + \rho_1)^2 |A - A_1|^2 \\ \leq \bar{K}_4 |A - A_1|^2. \end{cases} \tag{44}$$

$$\begin{cases} |H_{15}(t, I) - H_{15}(t, I_1)|^2 = |(1 - q)\delta E - (\mu + d + \rho)I - (1 - q)\delta E + (\mu + d + \rho)I_1|^2, \\ = | - (\mu + d + \rho)(I - I_1)|^2, \\ \leq 4(\mu + d + \rho)^2 |I - I_1|^2 \\ \leq \bar{K}_5 |I - I_1|^2. \end{cases} \tag{45}$$

$$\begin{cases} |H_{16}(t, R) - H_{16}(t, R_1)|^2 = |\rho I + \rho_1 A - (\kappa + \mu)R - \rho I + \rho_1 A + (\kappa + \mu)R_1|^2, \\ = | - (\kappa + \mu)(R - R_1)|^2, \\ \leq 4(\kappa + \mu)^2 |R - R_1|^2 \\ \leq \bar{K}_6 |R - R_1|^2. \end{cases} \tag{46}$$

$$\begin{cases} |H_{11}(t, S) - H_{11}(t, S_1)|^2 = \frac{3}{2} \nu_1^2 |S - S_1|^2 \leq \bar{K}_1 |S - S_1|^2, \\ |H_{12}(t, V) - H_{12}(t, V_1)|^2 = \frac{3}{2} \nu_2^2 |V - V_1|^2 \leq \bar{K}_2 |V - V_1|^2, \\ |H_{13}(t, E) - H_{13}(t, E_1)|^2 = \frac{3}{2} \nu_3^2 |E - E_1|^2 \leq \bar{K}_3 |E - E_1|^2, \\ |H_{14}(t, A) - H_{14}(t, A_1)|^2 = \frac{3}{2} \nu_4^2 |A - A_1|^2 \leq \bar{K}_4 |A - A_1|^2, \\ |H_{15}(t, I) - H_{15}(t, I_1)|^2 = \frac{3}{2} \nu_5^2 |I - I_1|^2 \leq \bar{K}_5 |I - I_1|^2, \\ |H_{16}(t, R) - H_{16}(t, R_1)|^2 = \frac{3}{2} \nu_6^2 |R - R_1|^2 \leq \bar{K}_6 |R - R_1|^2. \end{cases} \tag{47}$$

We get the result if the condition given below is satisfied

$$\max \left\{ \frac{\frac{1}{N^2} \left( a_1^2 \|I^2\|_\infty + a_2^2 \|A^2\|_\infty \right) + (\mu + \omega)^2}{K_1/3}, \frac{\frac{(1+\psi)^2}{N^2} \left( a_1^2 \|I(t)^2\|_\infty + a_2^2 \|A(t)^2\|_\infty \right) + (\theta + \mu)^2}{K_2/3}, \frac{(\delta + \mu)^2}{K_3/3}, \frac{(\rho_1 + \mu)^2}{K_4/3}, \frac{(\rho + \mu + d)^2}{K_5/3}, \frac{(\kappa + \mu)^2}{K_6/3} \right\} < 1.$$

**Numerical scheme for the model using Atangana-Baleanu derivative**

Now consider the case where the differential operator is Atangana-Baleanu. The following results are presented:

$$S(t) = \mathcal{A}H_{11}(S, \tau) + \mathcal{A}\nu_1 H_1(S, \tau)\dot{W}_0(\tau) + \mathcal{B} \int_0^t \mathcal{C}H_{11}(S, \tau)d\tau + \mathcal{B} \int_0^t \mathcal{C}H_1(S, \tau)\nu_1 \dot{W}_0(\tau)d\tau + S(0), \tag{48}$$

$$V(t) = \mathcal{A}H_{12}(V, \tau) + \mathcal{A}\nu_2 H_2(V, \tau)\dot{W}_1(\tau) + \mathcal{B} \int_0^t \mathcal{C}H_{12}(V, \tau)d\tau + \mathcal{B} \int_0^t \mathcal{C}H_2(V, \tau)\nu_2\dot{W}_1(\tau)d\tau + V(0), \quad (49)$$

$$E(t) = \mathcal{A}H_{13}(E, \tau) + \mathcal{A}\nu_3 H_3(E, \tau)\dot{W}_2(\tau) + \mathcal{B} \int_0^t \mathcal{C}H_{13}(E, \tau)d\tau + \mathcal{B} \int_0^t \mathcal{C}H_3(E, \tau)\nu_3\dot{W}_2(\tau)d\tau + E(0), \quad (50)$$

$$A(t) = \mathcal{A}H_{14}(A, \tau) + \mathcal{A}\nu_4 H_4(A, \tau)\dot{W}_3(\tau) + \mathcal{B} \int_0^t \mathcal{C}H_{14}(A, \tau)d\tau + \mathcal{B} \int_0^t \mathcal{C}H_4(A, \tau)\nu_4\dot{W}_3(\tau)d\tau + A(0), \quad (51)$$

$$I(t) = \mathcal{A}H_{15}(I, \tau) + \mathcal{A}\nu_5 H_5(I, \tau)\dot{W}_4(\tau) + \mathcal{B} \int_0^t \mathcal{C}H_{15}(I, \tau)d\tau + \mathcal{B} \int_0^t \mathcal{C}H_5(I, \tau)\nu_5\dot{W}_4(\tau)d\tau + I(0), \quad (52)$$

$$R(t) = \mathcal{A}H_{16}(R, \tau) + \mathcal{A}\nu_6 H_6(R, \tau)\dot{W}_5(\tau) + \mathcal{B} \int_0^t \mathcal{C}H_{16}(R, \tau)d\tau + \mathcal{B} \int_0^t \mathcal{C}H_6(R, \tau)\nu_6\dot{W}_5(\tau)d\tau + R(0), \quad (53)$$

where  $\mathcal{C} = (t - \tau)^{\zeta-1}$ . Here the function  $H_{11}$  and  $H_1$  are approximately using the Lagrange Polynomials taken from<sup>43</sup>. This yields to:

$$\begin{aligned} S(t_{n+1}) = & \mathcal{A}H_{11}(S_n, t_n) + \mathcal{A}\nu_1 H_1(S_n, t_n)[W_0(t_{n+1}) - W_0(t_n)] + \mathcal{B}_1 \sum_{g=2}^n H_{11}(S_{g-2}, t_{g-2})M_{01} \\ & + \mathcal{B}_2 \sum_{g=2}^n \left\{ H_{11}(S_{g-1}, t_{g-1}) - H_{11}(S_{g-2}, t_{g-2}) \right\} M_{02} + \mathcal{B}_3 \sum_{g=2}^n \left\{ H_{11}(S_g, t_g) - 2H_{11}(S_{g-1}, t_{g-1}) \right. \\ & \left. + H_{11}(S_{g-2}, t_{g-2}) \right\} \times M_{03} + \mathcal{B}_1\nu_1 \sum_{g=2}^n H_1(S_{g-2}, t_{g-2})M_{01}[W_0(t_{g-1}) - W_0(t_{g-2})] + \mathcal{B}_2\nu_1 \\ & \sum_{g=2}^n \left\{ H_1(S_{g-1}, t_{g-1})[W_0(t_g) - W_0(t_{g-1})] - H_1(S_{g-2}, t_{g-2})[W_0(t_{g-1}) - W_0(t_{g-2})] \right\} M_{02} \\ & + \mathcal{B}_3\nu_1 \sum_{g=2}^n \left\{ H_1(S_g, t_g)[W_0(t_{g+1}) - W_0(t_g)] - 2H_1(S_{g-1}, t_{g-1})[W_0(t_g) - W_0(t_{g-1})] \right. \\ & \left. + H_1(S_{g-2}, t_{g-2})[W_0(t_{g-1}) - W_0(t_{g-2})] \right\} M_{03}, \end{aligned} \quad (54)$$

where  $\mathcal{B}_1 = \frac{\zeta(\Delta t)^{\zeta-1}}{AB(\zeta)\Gamma(\zeta+1)}$ ,  $\mathcal{B}_2 = \frac{\zeta(\Delta t)^{\zeta-1}}{AB(\zeta)\Gamma(\zeta+2)}$  and  $\mathcal{B}_3 = \frac{\zeta(\Delta t)^{\zeta-1}}{AB(\zeta)\Gamma(\zeta+3)}$ ,

$$\begin{aligned} V(t_{n+1}) = & \mathcal{A}H_{12}(V_n, t_n) + \mathcal{A}\nu_2 H_2(V_n, t_n)[W_1(t_{n+1}) - W_1(t_n)] + \mathcal{B}_1 \sum_{g=2}^n H_{12}(V_{g-2}, t_{g-2})M_{01} \\ & + \mathcal{B}_2 \sum_{g=2}^n \left\{ H_{12}(V_{g-1}, t_{g-1}) - H_{12}(V_{g-2}, t_{g-2}) \right\} M_{02} + \mathcal{B}_3 \sum_{g=2}^n \left\{ H_{12}(V_g, t_g) - 2H_{12}(V_{g-1}, t_{g-1}) \right. \\ & \left. + H_{12}(V_{g-2}, t_{g-2}) \right\} \times M_{03} + \mathcal{B}_1\nu_2 \sum_{g=2}^n H_2(V_{g-2}, t_{g-2})M_{01}[W_1(t_{g-1}) - W_1(t_{g-2})] + \mathcal{B}_2\nu_2 \\ & \sum_{g=2}^n \left\{ H_2(V_{g-1}, t_{g-1})[W_1(t_g) - W_1(t_{g-1})] - H_2(V_{g-2}, t_{g-2})[W_1(t_{g-1}) - W_1(t_{g-2})] \right\} M_{02} \\ & + \mathcal{B}_3\nu_2 \sum_{g=2}^n \left\{ H_2(V_g, t_g)[W_1(t_{g+1}) - W_1(t_g)] - 2H_2(V_{g-1}, t_{g-1})[W_1(t_g) - W_1(t_{g-1})] \right. \\ & \left. + H_2(V_{g-2}, t_{g-2})[W_1(t_{g-1}) - W_1(t_{g-2})] \right\} M_{03}, \end{aligned} \quad (55)$$

$$\begin{aligned}
E(t_{n+1}) = & \mathcal{A}H_{13}(E_n, t_n) + \mathcal{A}\nu_3 H_3(E_n, t_n)[W_2(t_{n+1}) - W_2(t_n)] + \mathcal{B}_1 \sum_{g=2}^n H_{13}(E_{g-2}, t_{g-2})M_{01} \\
& + \mathcal{B}_2 \sum_{g=2}^n \left\{ H_{13}(E_{g-1}, t_{g-1}) - H_{13}(E_{g-2}, t_{g-2}) \right\} M_{02} + \mathcal{B}_3 \sum_{g=2}^n \left\{ H_{13}(E_g, t_g) - 2H_{13}(E_{g-1}, t_{g-1}) \right. \\
& \left. + H_{13}(E_{g-2}, t_{g-2}) \right\} \times M_{03} + \mathcal{B}_1\nu_3 \sum_{g=2}^n H_3(E_{g-2}, t_{g-2})M_{01}[W_2(t_{g-1}) - W_2(t_{g-2})] + \mathcal{B}_2\nu_3 \\
& \sum_{g=2}^n \left\{ H_3(E_{g-1}, t_{g-1})[W_2(t_g) - W_2(t_{g-1})] - H_3(E_{g-2}, t_{g-2})[W_2(t_{g-1}) - W_2(t_{g-2})] \right\} M_{02} \\
& + \mathcal{B}_3\nu_3 \sum_{g=2}^n \left\{ H_3(E_g, t_g)[W_2(t_{g+1}) - W_2(t_g)] - 2H_3(E_{g-1}, t_{g-1})[W_2(t_g) - W_2(t_{g-1})] \right. \\
& \left. + H_3(E_{g-2}, t_{g-2})[W_2(t_{g-1}) - W_2(t_{g-2})] \right\} M_{03},
\end{aligned} \tag{56}$$

$$\begin{aligned}
A(t_{n+1}) = & \mathcal{A}H_{14}(A_n, t_n) + \mathcal{A}\nu_4 H_4(A_n, t_n)[W_3(t_{n+1}) - W_3(t_n)] + \mathcal{B}_1 \sum_{g=2}^n H_{14}(A_{g-2}, t_{g-2})M_{01} \\
& + \mathcal{B}_2 \sum_{g=2}^n \left\{ H_{14}(A_{g-1}, t_{g-1}) - H_{14}(A_{g-2}, t_{g-2}) \right\} M_{02} + \mathcal{B}_3 \sum_{g=2}^n \left\{ H_{14}(A_g, t_g) - 2H_{14}(A_{g-1}, t_{g-1}) \right. \\
& \left. + H_{14}(A_{g-2}, t_{g-2}) \right\} \times M_{03} + \mathcal{B}_1\nu_4 \sum_{g=2}^n H_4(A_{g-2}, t_{g-2})M_{01}[W_3(t_{g-1}) - W_3(t_{g-2})] + \mathcal{B}_2\nu_4 \\
& \sum_{g=2}^n \left\{ H_4(A_{g-1}, t_{g-1})[W_3(t_g) - W_3(t_{g-1})] - H_4(A_{g-2}, t_{g-2})[W_3(t_{g-1}) - W_3(t_{g-2})] \right\} M_{02} \\
& + \mathcal{B}_3\nu_4 \sum_{g=2}^n \left\{ H_4(A_g, t_g)[W_3(t_{g+1}) - W_3(t_g)] - 2H_4(A_{g-1}, t_{g-1})[W_3(t_g) - W_3(t_{g-1})] \right. \\
& \left. + H_4(A_{g-2}, t_{g-2})[W_3(t_{g-1}) - W_3(t_{g-2})] \right\} M_{03},
\end{aligned} \tag{57}$$

$$\begin{aligned}
I(t_{n+1}) = & \mathcal{A}H_{15}(I_n, t_n) + \mathcal{A}\nu_5 H_5(I_n, t_n)[W_4(t_{n+1}) - W_4(t_n)] + \mathcal{B}_1 \sum_{g=2}^n H_{15}(I_{g-2}, t_{g-2})M_{01} \\
& + \mathcal{B}_2 \sum_{g=2}^n \left\{ H_{15}(I_{g-1}, t_{g-1}) - H_{15}(I_{g-2}, t_{g-2}) \right\} M_{02} + \mathcal{B}_3 \sum_{g=2}^n \left\{ H_{15}(I_g, t_g) - 2H_{15}(I_{g-1}, t_{g-1}) \right. \\
& \left. + H_{15}(I_{g-2}, t_{g-2}) \right\} \times M_{03} + \mathcal{B}_1\nu_5 \sum_{g=2}^n H_5(I_{g-2}, t_{g-2})M_{01}[W_4(t_{g-1}) - W_4(t_{g-2})] + \mathcal{B}_2\nu_5 \\
& \sum_{g=2}^n \left\{ H_5(I_{g-1}, t_{g-1})[W_4(t_g) - W_4(t_{g-1})] - H_5(I_{g-2}, t_{g-2})[W_4(t_{g-1}) - W_4(t_{g-2})] \right\} M_{02} \\
& + \mathcal{B}_3\nu_5 \sum_{g=2}^n \left\{ H_5(I_g, t_g)[W_4(t_{g+1}) - W_4(t_g)] - 2H_5(I_{g-1}, t_{g-1})[W_4(t_g) - W_4(t_{g-1})] \right. \\
& \left. + H_5(I_{g-2}, t_{g-2})[W_4(t_{g-1}) - W_4(t_{g-2})] \right\} M_{03},
\end{aligned} \tag{58}$$

$$\begin{aligned}
 R(t_{n+1}) = & \mathcal{A}H_{16}(R_n, t_n) + \mathcal{A}\nu_6 H_6(R_n, t_n)[W_5(t_{n+1}) - W_5(t_n)] + \mathcal{B}_1 \sum_{g=2}^n H_{16}(R_{g-2}, t_{g-2})M_{01} \\
 & + \mathcal{B}_2 \sum_{g=2}^n \left\{ H_{16}(R_{g-1}, t_{g-1}) - H_{16}(R_{g-2}, t_{g-2}) \right\} M_{02} + \mathcal{B}_3 \sum_{g=2}^n \left\{ H_{16}(R_g, t_g) - 2H_{16}(R_{g-1}, t_{g-1}) \right. \\
 & \left. + H_{16}(R_{g-2}, t_{g-2}) \right\} \times M_{03} + \mathcal{B}_1\nu_6 \sum_{g=2}^n H_6(R_{g-2}, t_{g-2})M_{01}[W_5(t_{g-1}) - W_5(t_{g-2})] + \mathcal{B}_2\nu_6 \\
 & \sum_{g=2}^n \left\{ H_6(R_{g-1}, t_{g-1})[W_5(t_g) - W_5(t_{g-1})] - H_6(R_{g-2}, t_{g-2})[W_5(t_{g-1}) - W_5(t_{g-2})] \right\} M_{02} \\
 & + \mathcal{B}_3\nu_6 \sum_{g=2}^n \left\{ H_6(R_g, t_g)[W_5(t_{g+1}) - W_5(t_g)] - 2H_6(R_{g-1}, t_{g-1})[W_5(t_g) - W_5(t_{g-1})] \right. \\
 & \left. + H_6(R_{g-2}, t_{g-2})[W_5(t_{g-1}) - W_5(t_{g-2})] \right\} M_{03},
 \end{aligned} \tag{59}$$

where  $M_{01} = [(n - g + 1)^\zeta - (n - g)^\zeta]$

$$\begin{aligned}
 M_{02} = & \left[ (n - g + 1)^\zeta (n - g + 3 + 2\zeta) - (n - g)^\zeta (n - g + 3 + 3\zeta) \right] \\
 M_{03} = & \left[ (n - g + 1)^\zeta \left[ 2(n - g)^2 + (3\zeta + 10)(n - g) + 2\zeta^2 + 9\zeta + 12 \right] - (n - g)^\zeta \left[ 2(n - g)^2 + (5\zeta + 10)(n - g) + 6\zeta^2 + 18\zeta + 12 \right] \right]
 \end{aligned}$$

### Numerical simulations

Using the numerical scheme described earlier, we present numerical simulations for different values of the fractional-order  $\zeta$ . For all simulations, a fixed temporal step size of  $h = 0.01$  was used to ensure numerical stability and to accurately capture the system's dynamics. Both the deterministic and stochastic schemes were confirmed to converge robustly to the true steady-state solutions.

The baseline numerical values for the model parameters are taken from Table 1. The constants for the stochastic noise terms are set to  $\nu_1 = 2 \times 10^{-4}$  and  $\nu_i = 2 \times 10^{-2}$  for  $i = 2, \dots, 6$ .

Specifically, the results shown in Figs. 4 to 9 correspond to the Disease-Free Equilibrium (DFE) case, simulated with the following parameter values:  $\mu = 1/(67.7 \times 365)$ ,  $\Pi = \mu \times 230557367$ ,  $a_1 = 0.8983$ ,  $a_2 = 0.3827$ ,  $\omega = 0.01$ ,  $\kappa = 0.3129$ ,  $\delta = 0.9982$ ,  $q = 0.9931$ ,  $\rho_1 = 0.3028$ ,  $\rho = 0.7926$ ,  $d = 0.6784$ ,  $\theta = 0.01$ ,  $\psi = 0.6$ , and the aforementioned noise constants  $\nu_1 - \nu_6$ , using a step size of  $h = 0.01$ .

We provide simulation results in Figs. 4 to 16. Figure 4 compares the susceptible compartment  $S(t)$  for the fractional-order and stochastic fractional-order systems across various values of  $\zeta$ . Figure 5 presents a similar comparison for the vaccinated compartment  $V(t)$ . Likewise, Figs. 6 to 9 show the comparison for the exposed ( $E$ ), asymptomatic ( $A$ ), infected ( $I$ ), and recovered ( $R$ ) compartments, respectively. These results demonstrate that the solution converges to the disease-free equilibrium (DFE).

Figures 10 to 15 represent the model solutions for the fractional and stochastic fractional differential equations. The results show that the solutions approach the endemic equilibrium (EE) point. The parameter values used in these simulations (Figures 10–15) are:

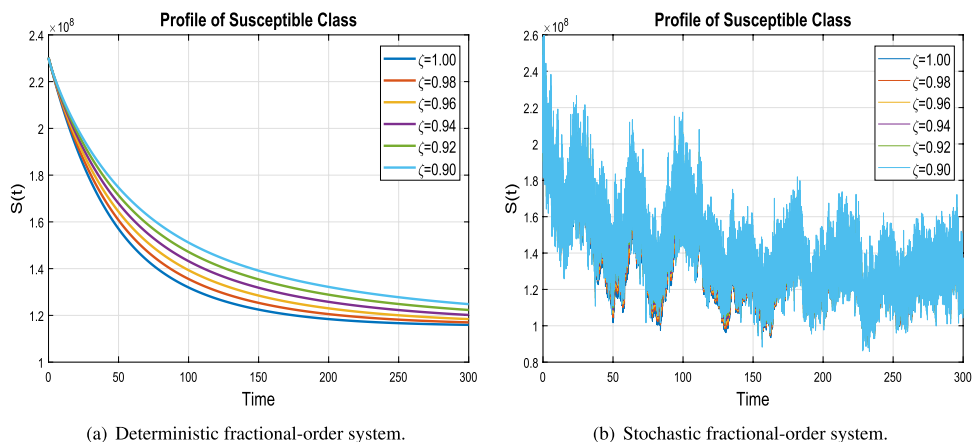


**Fig. 4.** Comparison of the susceptible compartment  $S(t)$  for different values of the fractional-order  $\zeta$ . Parameters for the Disease-Free Equilibrium (DFE) case:  $\mu = 1/(67.7 \times 365)$ ,  $\Pi = \mu \times 230557367$ ,  $a_1 = 0.8983$ ,  $a_2 = 0.3827$ ,  $\omega = 0.01$ ,  $\kappa = 0.3129$ ,  $\delta = 0.9982$ ,  $q = 0.9931$ ,  $\rho_1 = 0.3028$ ,  $\rho = 0.7926$ ,  $d = 0.6784$ ,  $\theta = 0.01$ ,  $\psi = 0.6$ ,  $\nu_1 = 2 \times 10^{-4}$ ,  $\nu_i = 0.02$  (for  $i = 2, \dots, 6$ ).

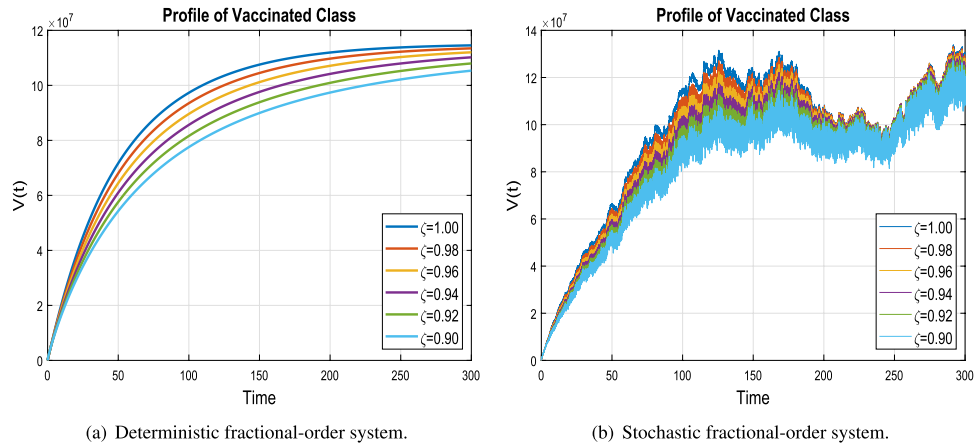


**Fig. 5.** Comparison of the vaccinated compartment  $V(t)$  for different values of  $\zeta$ . Parameters are the same as in Fig. 4 for the DFE case.

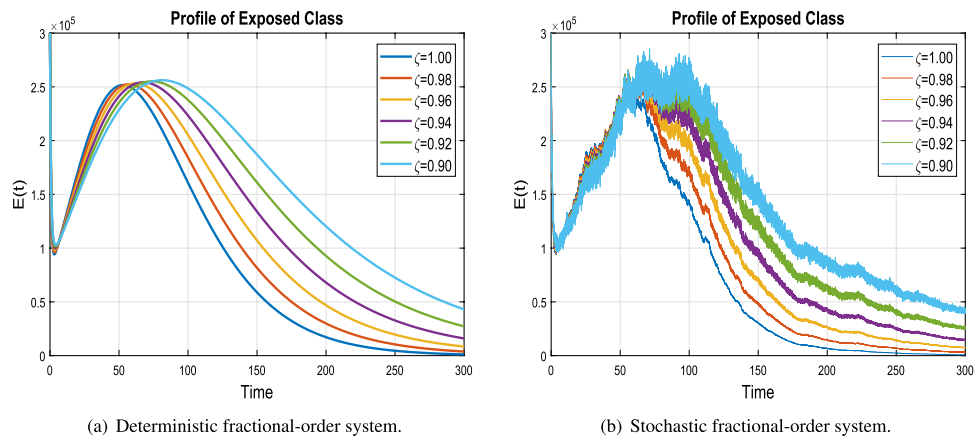


**Fig. 6.** Comparison of the exposed compartment  $E(t)$  for different values of  $\zeta$ . Parameters are the same as in Fig. 4 for the DFE case.

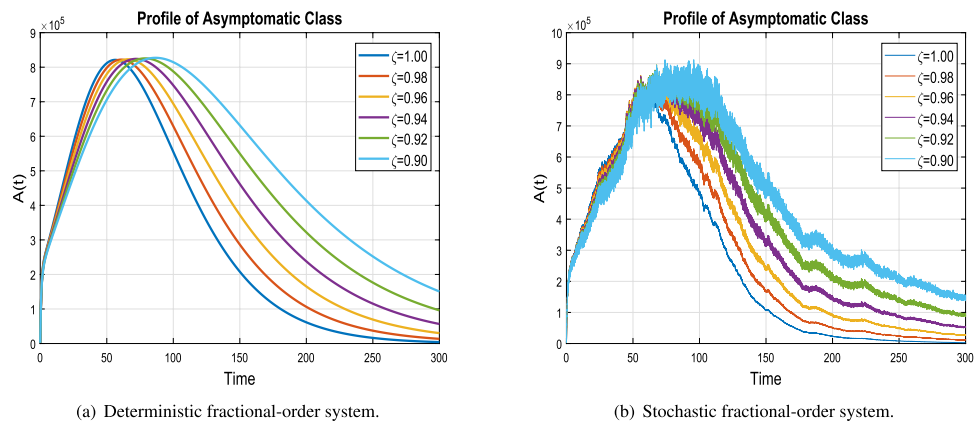


**Fig. 7.** Comparison of the asymptomatic infected compartment  $A(t)$  for different values of  $\zeta$ . Parameters are the same as in Fig. 4 for the DFE case.

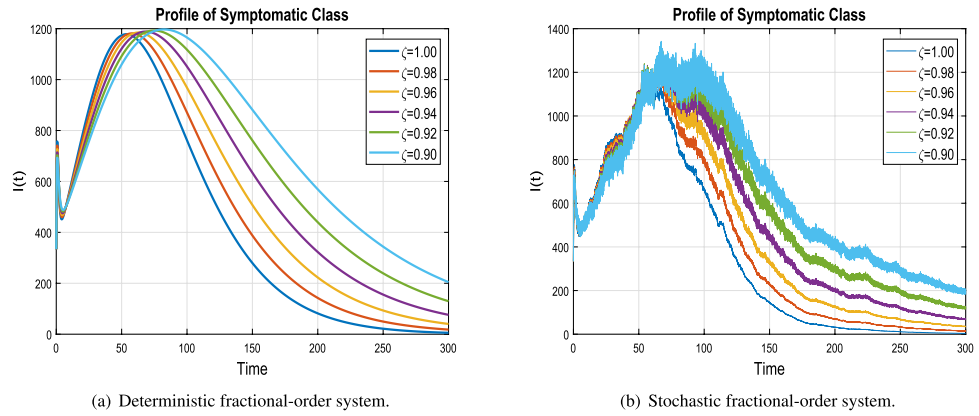


**Fig. 8.** Comparison of the symptomatic infected compartment  $I(t)$  for different values of  $\zeta$ . Parameters are the same as in Fig. 4 for the DFE case.

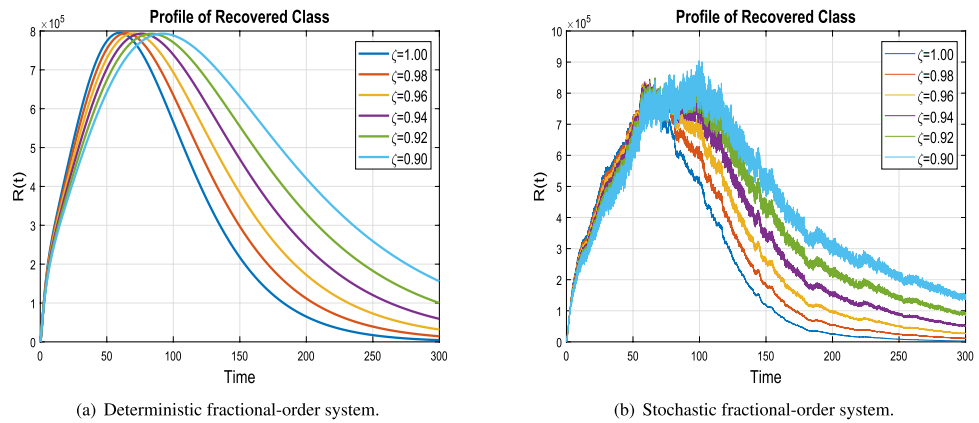


**Fig. 9.** Comparison of the recovered compartment  $R(t)$  for different values of  $\zeta$ . Parameters are the same as in Fig. 4 for the DFE case.

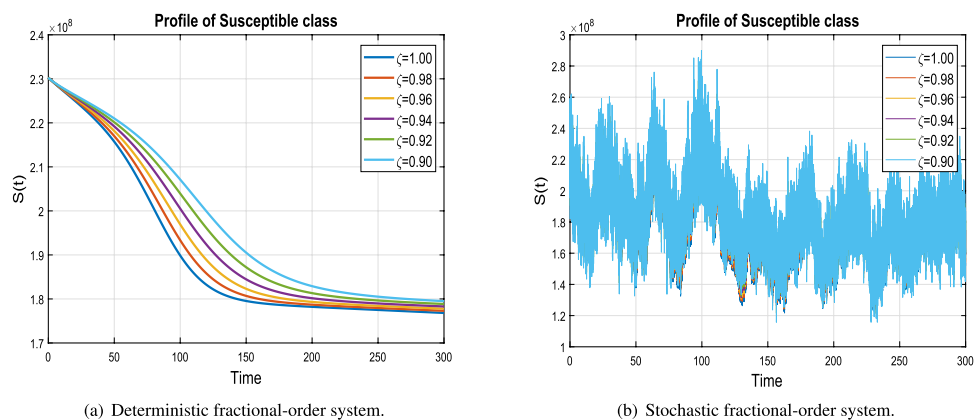


**Fig. 10.** Comparison of the susceptible compartment  $S(t)$  for different values of the fractional-order  $\zeta$ . Parameters for the Endemic Equilibrium (EE) case:  $\mu = 1/(67.7 \times 365)$ ,  $\Pi = \mu \times 230557367$ ,  $a_1 = 0.8983$ ,  $a_2 = 0.3827$ ,  $\omega = 0.001$ ,  $\kappa = 0.3129$ ,  $\delta = 0.9982$ ,  $q = 0.9931$ ,  $\rho_1 = 0.3028$ ,  $\rho = 0.7926$ ,  $d = 0.6784$ ,  $\theta = 0.01$ ,  $\psi = 0.6$ ,  $\nu_1 = 2 \times 10^{-4}$ ,  $\nu_i = 0.02$  (for  $i = 2, \dots, 6$ ).

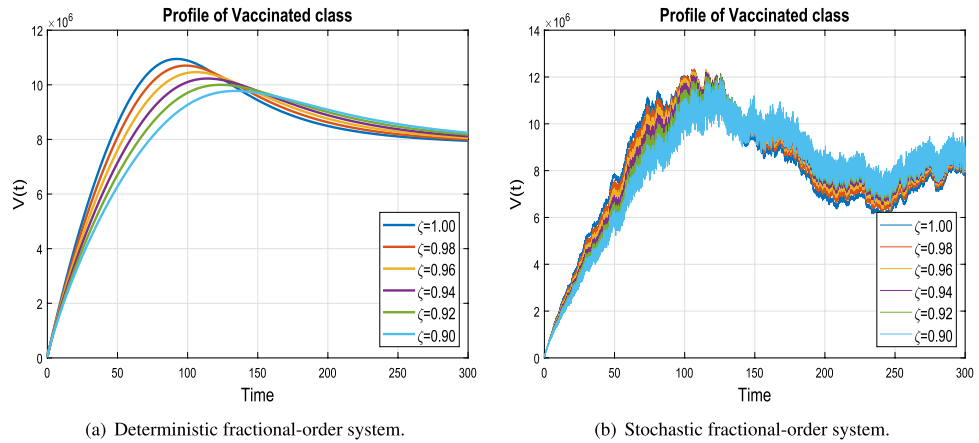


**Fig. 11.** Comparison of the vaccinated compartment  $V(t)$  for different values of  $\zeta$ . Parameters are the same as in Fig. 10 for the EE case.

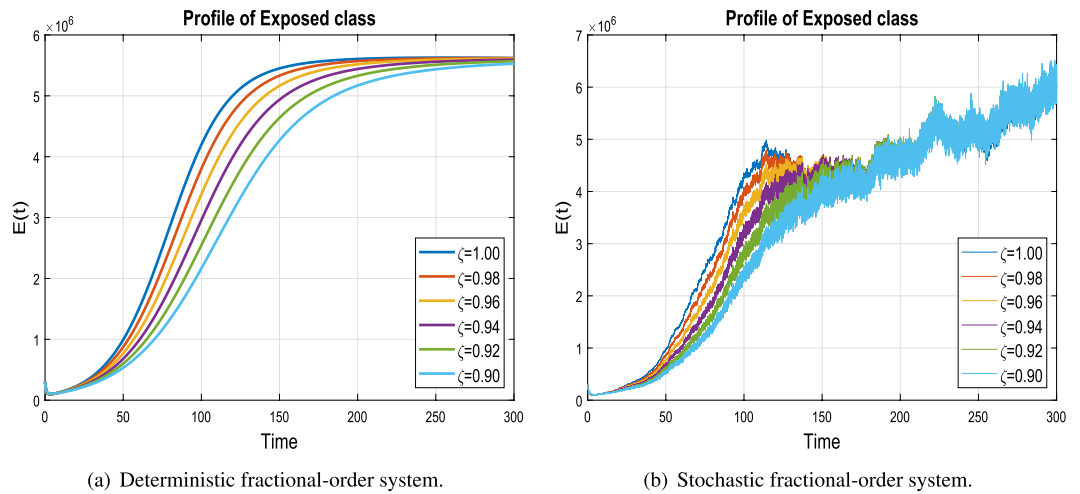


**Fig. 12.** Comparison of the exposed compartment  $E(t)$  for different values of  $\zeta$ . Parameters are the same as in Fig. 10 for the EE case.

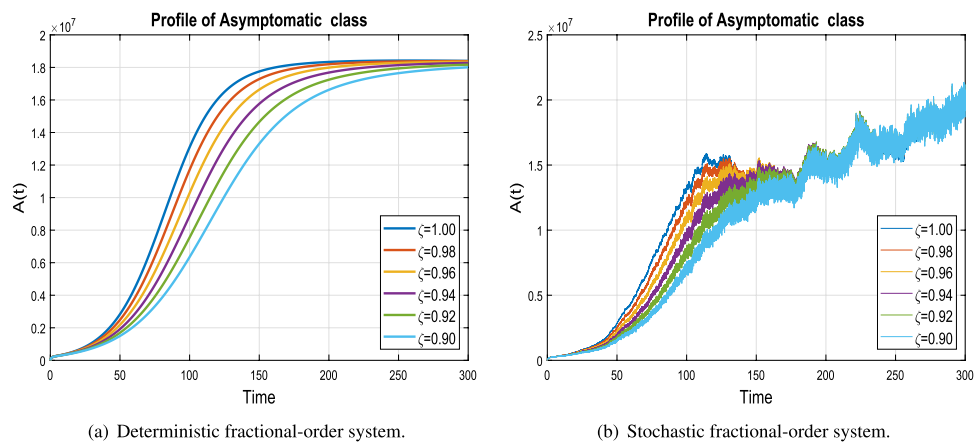


**Fig. 13.** Comparison of the asymptomatic infected compartment  $A(t)$  for different values of  $\zeta$ . Parameters are the same as in Fig. 10 for the EE case.

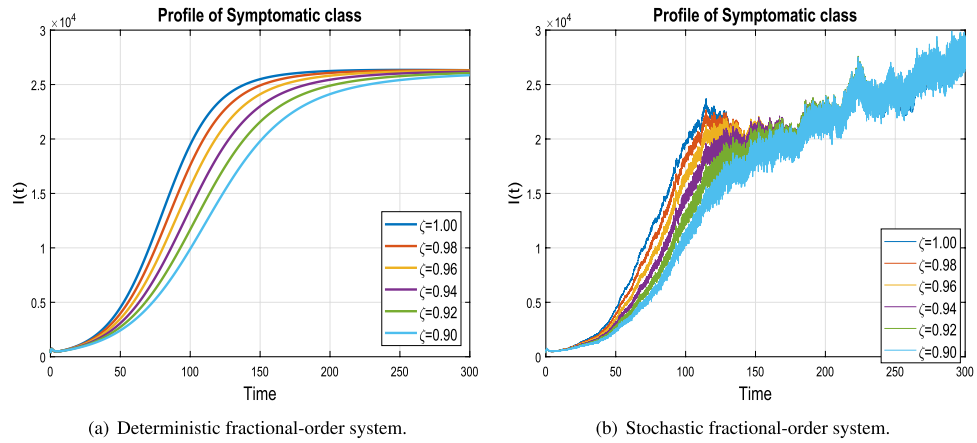


**Fig. 14.** Comparison of the symptomatic infected compartment  $I(t)$  for different values of  $\zeta$ . Parameters are the same as in Fig. 10 for the EE case.

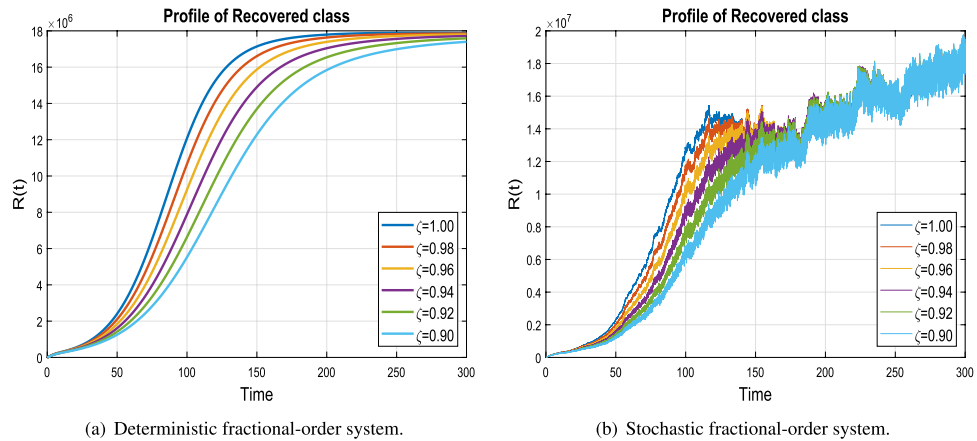


**Fig. 15.** Comparison of the recovered compartment  $R(t)$  for different values of  $\zeta$ . Parameters are the same as in Fig. 10 for the EE case.

$$\begin{aligned} \mu &= 1/(67.7 \times 365), \quad \Pi = \mu \times 230557367, \quad a_1 = 0.8983, \quad a_2 = 0.3827, \\ \omega &= 0.001, \quad \kappa = 0.3129, \quad \delta = 0.9982, \quad q = 0.9931, \\ \rho_1 &= 0.3028, \quad \rho = 0.7926, \quad d = 0.6784, \quad \theta = 0.01, \quad \psi = 0.6, \\ \nu_1 &= 2 \times 10^{-4}, \quad \nu_2 = 2 \times 10^{-2}, \quad \nu_3 = 2 \times 10^{-2}, \\ \nu_4 &= 2 \times 10^{-2}, \quad \nu_5 = 2 \times 10^{-2}, \quad \nu_6 = 2 \times 10^{-2}, \end{aligned}$$

with a step size of  $h = 0.01$ .

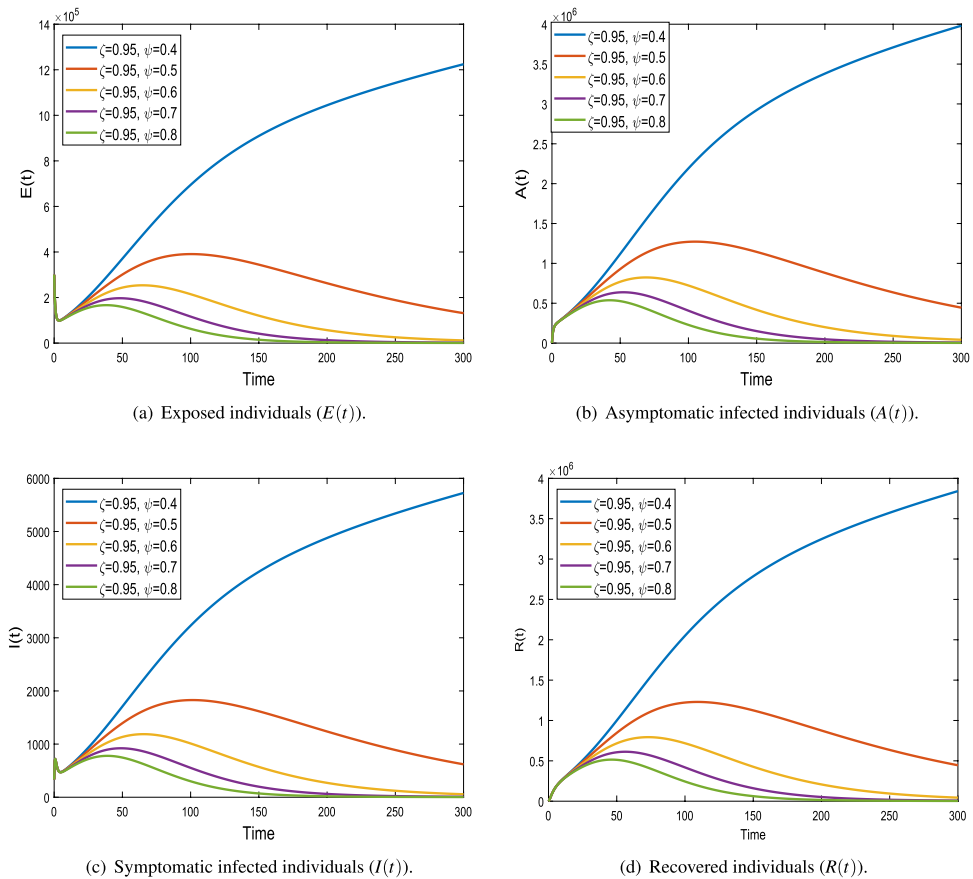
The variation in the fractional-order  $\zeta$  correctly captures both the disease-free equilibrium (DFE) and endemic equilibrium (EE) solution behaviors, which is characteristic of fractional model simulations.

Figure 16 shows the impact of the vaccine efficacy rate  $\psi$  for a fixed fractional-order  $\zeta = 0.95$ . As the vaccine efficacy  $\psi$  decreases, the population sizes of the model compartments change accordingly.

### Conclusion

In the present work, we formulated a mathematical model for COVID-19 infection using fractional differential equations with the Mittag-Leffler kernel, which effectively captures the memory effects in disease dynamics. The model was further extended into a fractional stochastic differential equation framework to account for random fluctuations and uncertainty inherent in real world epidemic spread.

We established the positivity and boundedness of the model and derived its equilibrium points in the fractional deterministic case. The existence and uniqueness of solutions to the FSDE were rigorously proven, and a new numerical scheme tailored to the Atangana–Baleanu-type fractional stochastic model was proposed and implemented. The real COVID-19 data from Pakistan for the specified period were used to estimate realistic



**Fig. 16.** Impact of the vaccine efficacy rate ( $\psi$ ) on the system compartments for a fixed fractional-order  $\zeta = 0.95$ . Parameters:  $\mu = 1/(67.7 \times 365)$ ,  $\Pi = \mu \times 230557367$ ,  $a_1 = 0.8983$ ,  $a_2 = 0.3827$ ,  $\omega = 0.01$ ,  $\kappa = 0.3129$ ,  $\delta = 0.9982$ ,  $q = 0.9931$ ,  $\rho_1 = 0.3028$ ,  $\rho = 0.7926$ ,  $d = 0.6784$ ,  $\theta = 0.01$ .

parameter values. Simulations were carried out to examine the influence of the fractional-order parameter and other key parameters on disease dynamics, particularly their role in disease elimination scenarios.

The novelty of this study lies in the integration of fractional calculus in the Mittag-Leffler sense with stochastic modeling, offering a more realistic and flexible framework for capturing both memory effects and randomness in COVID-19 dynamics. This approach enhances the ability to simulate and understand the impact of fractional dynamics on control strategies, including vaccination.

This research provides a foundation for several important extensions. Future work will focus on incorporating spatial heterogeneity to analyze geographic variation in transmission and intervention efficacy. Furthermore, the model will be extended to include additional compartments, particularly a vaccinated-but-susceptible class, to more accurately represent waning immunity and breakthrough infections.

## Data availability

Data is available from Refs [33, 34].

Received: 27 June 2025; Accepted: 2 September 2025

Published online: 26 September 2025

## References

- Zafar, Z. U. A. et al. Impact of public health awareness programs on covid-19 dynamics: a fractional modeling approach. *Fractals* **31**, 2340005-1-2340005-20 (2023).
- Butt, A., Ahmad, W., Rafiq, M. & Baleanu, D. Numerical analysis of atangana-baleanu fractional model to understand the propagation of a novel corona virus pandemic. *Alex. Eng. J.* **61**, 7007–7027. <https://doi.org/10.1016/j.aej.2021.12.042> (2022).
- Agusto, F. B. et al. Impact of public sentiments on the transmission of covid-19 across a geographical gradient. *PeerJ* **11**(e14736), 1–32. <https://doi.org/10.7717/peerj.14736> (2023).
- Khan, M. A. & Atangana, A. Modeling the dynamics of novel coronavirus (2019-ncov) with fractional derivative. *Alex. Eng. J.* **59**, 2379–2389 (2020).
- Ullah, S. & Khan, M. A. Modeling the impact of non-pharmaceutical interventions on the dynamics of novel coronavirus with optimal control analysis with a case study. *Chaos, Solitons & Fractals* **139**(110075), 1–15 (2020).
- Logeswari, K., Ravichandran, C. & Nisar, K. S. Mathematical model for spreading of covid-19 virus with the mittag-leffler kernel. *Numer. Methods Partial Differ. Equ.* **40**, e22652 (2024).

7. Iwa, L. L., Omame, A. & Chioma, S. A fractional-order model of covid-19 and malaria co-infection. *Bull. Biomath.* **2**, 133–161 (2024).
8. Kumar, P., SM, S. & Govindaraj, V. Forecasting of hiv/aids in south africa using 1990 to 2021 data: novel integer-and fractional-order fittings. *Int. J. Dyn. Control.* **12**, 2247–2263 (2024).
9. Ahmad, A., Farman, M., Sultan, M., Ahmad, H. & Askar, S. Analysis of hybrid nar-rbfs networks for complex non-linear covid-19 model with fractional operators. *BMC Infect. Dis.* **24**, 1051 (2024).
10. Rihan, F. & Alsakaji, H. Dynamics of a stochastic delay differential model for covid-19 infection with asymptomatic infected and interacting people: Case study in the uae. *Results Phys.* **28**, 104658 (2021).
11. Liu, X., Ullah, S., Alshehri, A. & Altanji, M. Mathematical assessment of the dynamics of novel coronavirus infection with treatment: A fractional study. *Chaos, Solitons & Fractals* **153**, 111534 (2021).
12. Beigi, A. et al. Application of reinforcement learning for effective vaccination strategies of coronavirus disease 2019 (covid-19). *Eur. Phys. J. Plus* **136**, 1–22 (2021).
13. Pandey, P., Gómez-Aguilar, J. F., Kaabar, M. K., Siri, Z. & Abd Allah, A. M. Mathematical modeling of covid-19 pandemic in india using caputo-fabrizio fractional derivative. *Comput. Biol. Med.* **145**, 105518 (2022).
14. He, Y. & Wang, Z. Stability analysis and optimal control of a fractional cholera epidemic model. *Fractal Fract.* **6**, 157 (2022).
15. Okyere, S. & Ackora-Prah, J. Modeling and analysis of monkeypox disease using fractional derivatives. *Results Eng.* **17**, 100786 (2023).
16. Aba Oud, M. A. et al. A fractional order mathematical model for covid-19 dynamics with quarantine, isolation, and environmental viral load. *AAAdv. Differ. Equations* **2021**, 1–19 (2021).
17. Ullah, M. S., Higazy, M. & Kabir, K. A. Modeling the epidemic control measures in overcoming covid-19 outbreaks: A fractional-order derivative approach. *Chaos, Solitons & Fractals* **155**, 111636 (2022).
18. Paul, S. et al. A fractal-fractional order susceptible-exposed-infected-recovered (seir) model with caputo sense. *Healthc. Anal.* **5**, 100317 (2024).
19. Okyere, E., Adjei, E., Abidemi, A. & Asante-Asamani, M. Fractional order for the transmission dynamics of coffee berry diseases (cbd). *Eur. J. Appl. Math.* **32**, 1123–1148. <https://doi.org/10.1017/S095679252100018X> (2021).
20. Qiao, Y., Ding, Y., Pang, D., Wang, B. & Lu, T. Fractional-order modeling of covid-19 transmission dynamics: A study on vaccine immunization failure. *Mathematics* **12**, 3378 (2024).
21. Roberts, M., Andreasen, V., Lloyd, A. & Pellis, L. Nine challenges for deterministic epidemic models. *Epidemics* **10**, 49–53 (2015).
22. Shi, Z. & Jiang, D. Environmental variability in a stochastic hiv infection model. *Commun. Nonlinear Sci. Numer. Simul.* **120**, 107201 (2023).
23. Mangal, S., Bonyah, E., Sharma, V. S. & Yuan, Y. A novel fractional-order stochastic epidemic model to analyze the role of media awareness in the spread of conjunctivitis. *Healthc. Anal.* **5**, 100302 (2024).
24. Alkahtani, B. S. T. & Koca, I. Fractional stochastic sir model. *Results Phys.* **24**, 104124 (2021).
25. Cui, T., Liu, P. & Din, A. Fractal-fractional and stochastic analysis of norovirus transmission epidemic model with vaccination effects. *Sci. Rep.* **11**, 24360 (2021).
26. Rashid, S. & Jarad, F. Stochastic dynamics of the fractal-fractional ebola epidemic model combining a fear and environmental spreading mechanism. *AIMS Mathematics* **8**, 3634–3675 (2023).
27. Omar, O. A., Elbarkouky, R. A. & Ahmed, H. M. Fractional stochastic models for covid-19: Case study of egypt. *Results Phys.* **23**, 104018 (2021).
28. Sun, T.-C. et al. Mathematical modeling of covid-19 with vaccination using fractional derivative: A case study. *Fractal Fract.* **7** (2023).
29. Atangana, A. & Baleanu, D. New fractional derivatives with non-local and non-singular kernel: theory and application to heat transfer model. *Therm. Sci.* **20**, 763–769. <https://doi.org/10.2298/TSCI16011018A> (2016).
30. Baleanu, D., Jajarmi, A. & Hajipour, M. On the nonlinear dynamical systems within the generalized fractional derivatives with mittag-leffler kernel. *Nonlinear Dyn.* **94**, <https://doi.org/10.1007/s11071-018-4367-y> (2018).
31. Jose, S. et al. Computational dynamics of a fractional order substance addictions transfer model with atangana-baleanu-caputo derivative. *Math. Methods Appl. Sci.* **46**, n/a–n/a, <https://doi.org/10.1002/mma.8818> (2022).
32. Pakistan life expectancy 1950–2022. <https://www.macrotrends.net/countries/PAK/pakistan/life-expectancy> (2025). Accessed on August 2025.
33. Johns Hopkins University Center for Systems Science and Engineering. Covid-19 data for pakistan. <https://coronavirus.jhu.edu/region/pakistan>. Accessed: 2025-08-20.
34. Worldometer. Total coronavirus cases in pakistan. <https://www.worldometers.info/coronavirus/country/pakistan/> (2025). Accessed: August 2025.
35. Worldometer. Pakistan population. <https://www.worldometers.info/world-population> (2025). Accessed: August 2025.
36. Blower, S. & Dowlatabadi, H. Sensitivity and uncertainty analysis of complex models of disease transmission: An hiv model, as an example. *Int. Stat. Rev.* **62**, <https://doi.org/10.2307/1403510> (1994).
37. Wang, Y., Zhou, Y. & Heffernan, J. Viral dynamics model with ctl immune response incorporating antiretroviral therapy. *J. Math. Biol.* **67**, 901–934. <https://doi.org/10.1007/s00285-012-0580-3> (2013).
38. Wang, Y., Liu, J. & Heffernan, J. Viral dynamics of an htlv-i infection model with intracellular delay and ctl immune response delay. *J. Math. Anal. Appl.* **459**, <https://doi.org/10.1016/j.jmaa.2017.10.027> (2017).
39. Wang, Y., Liu, J. & Liu, L. Viral dynamics of an hiv model with latent infection incorporating antiretroviral therapy. *Adv. Differ. Equations* **2016**, 225. <https://doi.org/10.1186/s13662-016-0952-x> (2016).
40. Cariboni, J., Gatelli, D., Liska, R. & Saltelli, A. *The role of sensitivity analysis in ecological modelling*, vol. 203 (Elsevier, 2007).
41. Atangana, A. & Iqbal Araz, S. *Fractional Stochastic Differential Equations: Applications to Covid-19 Modeling* (2022).
42. Bonyah, E., Panigoro, H., Fatmawati, F., Rahmi, E. & Juga, M. Fractional stochastic modelling of monkeypox dynamics. *Results Control. Optim.* **12**, 100277. <https://doi.org/10.1016/j.rico.2023.100277> (2023).
43. Atangana, A. & Iqbal Araz, S. *New numerical Scheme With Newton Polynomial* (Academic Press, Elsevier, 2021).

## Acknowledgements

The authors express their gratitude to the Deanship of Scientific Research at King Khalid University for funding this work through the Large Research Group Project under grant number RGP.02/478/46.

## Author contributions

M.A.K., Z. U.A.Z. conceived the experiment(s), M.A.A., Z. U.A.Z., I.A conducted the experiment(s), M.A.K., E. A. and N.B.M.I. analysed the results. All authors reviewed the manuscript.

## Funding

No Funding.

## Declarations

### Competing interests

The authors declare no competing interests.

### Additional information

**Correspondence** and requests for materials should be addressed to M.A.K.

**Reprints and permissions information** is available at [www.nature.com/reprints](http://www.nature.com/reprints).

**Publisher's note** Springer Nature remains neutral with regard to jurisdictional claims in published maps and institutional affiliations.

**Open Access** This article is licensed under a Creative Commons Attribution-NonCommercial-NoDerivatives 4.0 International License, which permits any non-commercial use, sharing, distribution and reproduction in any medium or format, as long as you give appropriate credit to the original author(s) and the source, provide a link to the Creative Commons licence, and indicate if you modified the licensed material. You do not have permission under this licence to share adapted material derived from this article or parts of it. The images or other third party material in this article are included in the article's Creative Commons licence, unless indicated otherwise in a credit line to the material. If material is not included in the article's Creative Commons licence and your intended use is not permitted by statutory regulation or exceeds the permitted use, you will need to obtain permission directly from the copyright holder. To view a copy of this licence, visit <http://creativecommons.org/licenses/by-nc-nd/4.0/>.

© The Author(s) 2025